NONLINEAR OPTICAL PHENOMENA AND MATERIALS

*8554

Robert L. Byer
Department of Applied Physics, Stanford University, Stanford, California 94305

INTRODUCTION

The field of nonlinear optics has developed rapidly since its beginning in 1961. This development is in both the theory of nonlinear effects and the theory of nonlinear interactions in solids, and in the applications of nonlinear devices. This review discusses nonlinear interactions in solids and the resultant nonlinear coupling of electromagnetic waves that leads to second harmonic generation, optical mixing, and optical parametric oscillation. Material requirements for device applications are considered, and important nonlinear material properties summarized. At the outset, a brief review of the development of nonlinear optics and devices is in order to provide perspective of this rapidly growing field.

Historical Review

In 1961, shortly after the demonstration of the laser, Franken et al (1) generated the second harmonic of a Ruby laser in crystal quartz. The success of this experiment relied directly on the enormous increase of power spectral brightness provided by a laser source compared to incoherent sources. Power densities greater than 10^9 W/cm^2 became available; these correspond to an electric field strength of 10^6 V cm^{-1}. This field strength is comparable to atomic field strengths and, therefore, it was not too surprising that materials responded in a nonlinear manner to the applied fields.

The early work in nonlinear optics concentrated on second harmonic generation. Harmonic generation in the optical region is similar to the more familiar harmonic generation at radio frequencies, with one important exception. In the radio frequency range the wavelength is usually much larger than the harmonic generator, so that the interaction is localized in a volume much smaller than the dimensions of a wavelength. In the optical region the situation is usually reversed and the nonlinear medium extends over many wavelengths. This leads to the consideration of propagation effects since the electromagnetic wave interacts over an extended distance with the generated nonlinear polarization. The situation is similar to a propagating wave interacting with a phased linear dipole array. If this interaction is to be efficient,

the phase of the propagating wave and the generated polarization must be proper. In nonlinear optics this is referred to as phasematching. For second harmonic generation, phasematching implies that the phase velocity of the fundamental and second harmonic waves are equal in the nonlinear material. Since optical materials are dispersive, it is not possible to achieve equal phase velocities in isotropic materials. Shortly after Franken et al's first relatively inefficient nonphasematched second harmonic generation experiment, Kleinman (2), Giordmaine (3), and Maker et al (4), and later Akhmanov et al (5) showed that phase velocity matching could be achieved in birefringent crystals by using the crystal birefringence to offset the dispersion.

Along with the important concept of phasematching, other effects leading to efficient second harmonic generation were studied. These included focusing (6, 7), double refraction (8–10), and operation of second harmonic generators with an external resonator (11, 12) and within a laser cavity (13, 14).

An important extension of nonlinear interactions occurred in 1965 when Wang & Racette (15) observed significant gain in a three-frequency mixing experiment. The possibility of optical parametric gain had been previously considered theoretically by Kingston (16), Kroll (17), Akhmanov & Khokhlov (18), and Armstrong et al (19). It remained for Giordmaine & Miller (20) in 1965 to achieve adequate parametric gain in $LiNbO_3$ to overcome losses and reach threshold for coherent oscillation. This early work led to considerable activity in the study of parametric oscillators as tunable coherent light sources.

Simultaneously with the activity in nonlinear devices, the theory of nonlinear interactions received increased attention. It was recognized quite early that progress in the field depended critically upon the availability of quality nonlinear materials. Initially, the number of phasematchable nonlinear crystals with accurately measured nonlinear coefficients was limited to a handful of previously known piezoelectric, ferroelectric, or electro-optic materials. An important step in the problem of searching for new nonlinear materials was made when Miller (21) recognized that the nonlinear susceptibility was related to the third power of the linear susceptibility by a factor now known as Miller's delta. Whereas nonlinear coefficients of materials span over four orders of magnitude, Miller's delta is constant to within 50%. To the crystal grower and nonlinear materials scientist, this simple rule allows the prediction of nonlinear coefficients based on known crystal indices of refraction and symmetry, without having to carry out the expensive and time-consuming tasks of crystal growth, accurate measurement of the birefringence to predict phasematching, orientation, and finally second harmonic generation.

The early progress in nonlinear optics has been the subject of a number of monographs [Akhmanov & Khokhlov (22), Bloembergen (23), Butcher (24), Franken & Ward (25)] and review articles [Ovander (26), Bonch-Bruevich & Khodovoi (27), Minck et al (28), Pershan (28a), Akhmanov et al (29), Terhune & Maker (30), Akhmanov & Khokhlov (31), and Kielich (32)]. In addition, nonlinear materials have been reviewed by Suvorov & Sonin (33), Rez (34), and Hulme (34a), and a compilation of nonlinear materials is provided by Singh (35). Two books have appeared, one a brief introduction by Baldwin (36), and the second a clearly written

text by Zernike & Midwinter (37). Finally, a text covering all aspects of nonlinear optics is to appear soon (38).

Nonlinear Devices

The primary application of nonlinear materials is the generation of new frequencies not available with existing laser sources. The variety of applications for nonlinear optical devices is so large that I will touch only the highlights here.

Second harmonic generation (SHG) received early attention primarily because of early theoretical understanding and its use for measuring and testing the nonlinear properties of crystals. Efficient SHG has been demonstrated using a number of materials and laser sources. In 1968 Geusic et al (39) obtained efficient doubling of a continuous wave (cw) Nd:YAG laser using the crystal $Ba_2NaNb_5O_{15}$. That same year, Dowley (40) reported efficient SHG of an argon ion laser operating at 0.5145 μm in ADP. Later Hagen et al (41) reported 70% doubling efficiency of a high energy Nd:glass laser in KDP (potassium dihydrogen phosphate), and Chesler et al (42) reported efficient SHG of a Q-switch Nd:YAG laser using $LiIO_3$. An efficiently doubled Q-switched Nd:YAG laser is now available as a commercial laser source (43). In addition, $LiIO_3$ has been used to efficiently double a Ruby laser (44). Recently the 10.6 μm CO_2 laser has been doubled in Tellurium with 5% efficiency (45) and in a ternary semiconductor $CdGeAs_2$ with 15% efficiency (46).

Three-frequency nonlinear interactions include sum generation, difference frequency generation or mixing, and parametric generation and oscillation. An interesting application of sum generation is infrared up-conversion and image up-conversion. For example, Smith & Mahr (47) report achieving a detector noise equivalent power of 10^{-14} W at 3.5 μm by up-converting to 0.447 μm in $LiNbO_3$ using an argon ion laser pump source. This detection method is being used for infrared astronomy. Numerous workers have efficiently up-converted 10.6 μm to the visible range (48–52) for detection by a photomultiplier. An extension of single beam up-conversion is image up-conversion (37, 53, 54). Resolution to 300 lines has been achieved, but at a cost in up-conversion efficiency.

Combining two frequencies to generate the difference frequency by mixing was first demonstrated by Wang & Racette (15). Zernike & Berman (55) used this approach to generate tunable far infrared radiation. Recently a number of workers have utilized mixing in proustite (56, 57), CdSe (58), $ZnGeP_2$ (52, 52a), $AgGaS_2$ (59), and recently $AgGaSe_2$ (60, 61) to generate tunable coherent infrared output from near infrared or visible sources.

Perhaps the most unique aspect of nonlinear interactions is the generation of coherent continuously-tunable laser-like radiation by parametric oscillation in a nonlinear crystal. Parametric oscillators were well known in the microwave region (62, 63) prior to their demonstration in the optical range. To date, parametric oscillators have been tuned across the visible and near infrared in KDP (29, 64, 65) and ADP (66) when pumped at the second harmonic and fourth harmonic of the 1.06 μm Nd:YAG laser, and they have been tuned over the infrared range from 0.6 μm to 3.7 μm in $LiNbO_3$ (67–72). The above parametric oscillators were pumped by Q-switched, high peak power, laser sources. Parametric oscillators have

also been operated in a cw manner in $Ba_2NaNb_5O_{15}$ (73–76) and in $LiNbO_3$ (77, 78). However, the low gains inherent in cw pumping have held back research in this area.

In 1969 Harris (79) reviewed the theory and devices aspects of parametric oscillators. Up to that time oscillation had been achieved in only three materials: KDP, $LiNbO_3$, and $Ba_2NaNb_5O_{15}$. Since 1969 parametric oscillation has been extended to four new materials: ADP (80), $LiIO_3$ (81, 82), proustite (Ag_3AsS_3) (227), and CdSe (83). The new materials have extended the available tuning range. However, the development of oscillator devices still has remained materials limited. At this time $LiNbO_3$ is the only nonlinear crystal used in a commercially available parametric oscillator.[1] Smith (84) and recently Byer (85) have discussed parametric oscillators in review papers and Byer (86) has reviewed their application to infrared spectroscopy.

Nonlinear interactions allow the extension of coherent radiation by second harmonic generation, sum generation, and difference frequency mixing over a wavelength range from 2200 Å to beyond 1 mm in the far infrared. In addition, tunable coherent radiation can be efficiently generated from a fixed frequency pump laser source by parametric oscillation. The very wide spectral range and efficiency of nonlinear interactions assures that they will become increasingly important as coherent sources.

NONLINEAR PHENOMENA

Introduction

When a medium is subjected to an electric field the electrons in the medium are polarized. For weak electric fields the polarization is linearly proportional to the applied field

$$\mathbf{P} = \varepsilon_0 \chi^1 \mathbf{E}$$

where χ^1 is the linear optical susceptibility and ε_0 is the permittivity of free space with the value 8.85×10^{-12} F/m in mks units. The linear susceptibility is related to the medium's index of refraction n by $\chi^1 = n^2 - 1$.

In a crystalline medium the linear susceptibility is a tensor that obeys the symmetry properties of the crystal. Thus for isotropic media there is only one value of the index, and for uniaxial crystals two values, n_0 the ordinary and n_e the extraordinary indices of refraction, and for biaxial crystals three values n_α, n_β, and n_γ.

A linear polarizability is an approximation to the complete constitutive relation which can be written as an expansion in powers of the applied field, as

$$\mathbf{P} = \varepsilon_0[\chi^1 + \chi^2 \cdot \mathbf{E} + \chi^3 \cdot \mathbf{E}^2 + \ldots]\mathbf{E}$$

where χ^2 is the second order nonlinear susceptibility and χ^3 is the third order nonlinear susceptibility. A number of interesting optical phenomena arise from the second and third order susceptibilities. For example, χ^2 gives rise to second harmonic

[1] Chromatix Inc., Mountain View, California.

generation (1), dc rectification (87), the linear electro-optic effect or Pockels effect (25), parametric oscillation (20), and three-frequency processes such as mixing (15) and sum generation. The third order susceptibility is responsible for third harmonic generation (88), the quadratic electro-optic effect or Kerr effect (28), two-photon absorption (89), and Raman (90), Brillouin (91), and Rayleigh (92) scattering.

We are primarily interested in effects that arise from χ^2. For a review of the nonlinear susceptibility χ^2 and the resulting interactions in a nonlinear medium see Wemple & DiDomenico (93) and Ducuing & Flytzanis (93a).

To see how χ^2 gives rise to second harmonic generation and other nonlinear effects, consider an applied field

$$\mathbf{E} = \mathbf{E}_1 \cos(k_1 x - \omega t) + \mathbf{E}_2 \cos(k_2 x - \omega t)$$

incident on the nonlinear medium. The nonlinear polarization is proportional to $\chi^2\mathbf{E}^2$, giving

$$\tfrac{1}{2}\chi^2 \mathbf{E}_1^2[1 + \cos(2k_1 x - 2\omega_1 t)]$$

plus a similar term for frequency ω_2. This term describes both dc rectification and second harmonic generation. In addition, there are sum and mixing terms of the form

$$\chi^2 \mathbf{E}_1 \mathbf{E}_2[\cos\{(k_1 - k_2)x - (\omega_1 - \omega_2)t\} + \cos\{(k_1 + k_2)x - (\omega_1 + \omega_2)t\}]$$

present in the expansion. These terms describe difference frequency and sum frequency generation. All of the above processes take place simultaneously in the nonlinear medium. The question that naturally occurs is how one process is singled out to proceed efficiently relative to the competing processes. In nonlinear interactions phasematching selects the process of interest to the exclusion of the other possible processes. Thus, if the crystal birefringence is adjusted (by temperature or angle of propagation) such that second harmonic generation is the phasematched process, then it proceeds with relatively high efficiency compared to the remaining processes involving sum and difference frequency generation.

CRYSTAL SYMMETRY Like the linear susceptibility, the second order nonlinear susceptibility must display the symmetry properties of the crystal medium. An immediate consequence of this fact is that in centrosymmetric media the second order nonlinear coefficients must vanish. Thus nonlinear optical effects are restricted to acentric materials. This is the same symmetry requirement for the piezoelectric $\mathbf{d}$ tensors (94) and therefore the nonzero components of the second order susceptibility can be found by reference to the listed $\mathbf{d}$ tensors. However, the nonlinear coefficient tensors have been listed in a number of references (24, 35, 37, 95).

The tensor property of χ^2 can be displayed by writing the nonlinear polarization in the form

$$\mathbf{P}_i(\omega_3) = \varepsilon_0 \sum_{jk} \chi_{ijk} : E_j(\omega_2) E_k(\omega_1) \qquad 1.$$

where $\chi_{ijk}(-\omega_3, \omega_2, \omega_1)$ is the nonlinear susceptibility tensor.

In addition to crystal symmetry restrictions, χ_{ijk} satisfies two additional symmetry relations. The first is an intrinsic symmetry relation which can be derived for a lossless medium from general energy considerations (23, 96). This relation states that $\chi_{ijk}(-\omega_3, \omega_2, \omega_1)$ is invariant under any permutation of the three pairs of indices $(-\omega_3, i)$; (ω_2, j); (ω_1, k) as was first shown by Armstrong et al (19). The second symmetry relation is based on a conjecture by Kleinman (2) that in a lossless medium the permutation of the frequencies is irrelevant and therefore χ_{ijk} is symmetric under any permutation of its indices.

Finally, it is customary to use reduced notation and to write the nonlinear susceptibility in terms of a nonlinear coefficient $d_{ijk} = d_{im}$ where m runs from 1–6 with the correspondence

$$\begin{array}{lcccccc} (jk) = & (11) & (22) & (33) & (23) & (13) & (12) \\ m = & 1 & 2 & 3 & 4 & 5 & 6 \end{array}$$

and

$$P_i(\omega_3) = \varepsilon_0 \sum_{m=1}^{6} 2d_{im}(EE)_m \qquad 2.$$

The 3×6 d_{im} matrix operates on the column vector $(EE)_m$ given by

$$(EE)_1 = E_x^2; \quad (EE)_2 = E_y^2; \quad (EE)_3 = E_z^2;$$
$$(EE)_4 = 2E_yE_z; \quad (EE)_5 = 2E_xE_z; \quad (EE)_6 = 2E_xE_y$$

As an example, the nonlinear $\mathbf{d}$ tensor for the $\bar{4}2m$ point group to which KDP and the chalcopyrite semiconductor crystals belong has the components

$$P_x = 2d_{14}E_yE_z; \quad P_y = 2d_{14}E_xE_z; \quad P_z = 2d_{36}E_xE_y \qquad 3.$$

However, Kleinman's symmetry conjecture states that $d_{14} = d_{123}$ equals $d_{36} = d_{312}$ since any permutation of indices is allowed. This is experimentally verified. Equation 1 and 2 show that

$$\chi_{im}(-\omega_3, \omega_1, \omega_2) = 2d_{im}(-\omega_3, \omega_1, \omega_2) \qquad 4.$$

This defines the relation between the nonlinear susceptibility and the $\mathbf{d}$ coefficient used to describe second harmonic generation. The definition of the nonlinear susceptibility has been discussed in detail by Boyd & Kleinman (97) and by Bechmann & Kurtz (95).

MILLER'S RULE We have not yet made an estimate of the magnitude of the nonlinear susceptibility. An important step in estimating the magnitude of $\mathbf{d}$ was taken by Miller (21) when he proposed that the field could be written in terms of the polarization as

$$E(-\omega_3) = \frac{1}{\varepsilon_0} \sum_{jk} 2\Delta_{ijk}(-\omega_3, \omega_1, \omega_2)P_j(\omega_1)P_k(\omega_2) \qquad 5.$$

Comparing Equations 5 and 2 shows that the tensor $\mathbf{d}$ and Δ are related by

$$d_{ijk} = \varepsilon_0 \sum_{lmn} \chi_{il}(\omega_3)\chi_{jm}(\omega_2)\chi_{kn}(\omega_1)\Delta_{lmn}(-\omega_3, \omega_2, \omega_1) \qquad 6.$$

where $\chi_{ij} = (n_{ij}^2 - 1)$ relates the linear susceptibility to the index of refraction. Miller noted that Δ is remarkably constant for nonlinear materials even though $\mathbf{d}$ varies over four orders of magnitude.

Some insight into the physical significance of Δ can be gained by considering a simple anharmonic oscillator model representation of a crystal similar to the Drude-Lorentz model for valence electrons. This model has been previously discussed by Lax et al (98), Bloembergen (23), Garrett & Robinson (99), and Kurtz & Robinson (100). For simplicity we neglect the tensor character of the nonlinear effect and consider a scalar model. The anharmonic oscillator satisfies an equation

$$\ddot{x} + \Gamma\dot{x} + \omega_0^2 x + \alpha x^2 = \frac{e}{m} E(\omega, t)$$

where Γ is a damping constant, ω_0^2 is the resonant frequency in the harmonic approximation, and α is the anharmonic force constant. Here $E(\omega, t)$ is considered to be the local field in the medium. The linear approximation to the above equation has the well known solution

$$\chi(\omega) = n^2 - 1 = \omega_p^2/(\omega_0^2 - \omega^2 - i\Gamma\omega)$$

where $\omega_p^2 = Ne^2/m\varepsilon_0$ is the plasma frequency. Substituting the linear solution back into the anharmonic oscillator equation and solving for the nonlinear coefficient d in terms of the linear susceptibilities gives

$$d = \frac{Ne^3\alpha}{\varepsilon_0 m^2} \frac{1}{D(\omega_1)D(\omega_2)D(\omega_3)}$$

where $D(\omega)$ is the resonant denominator term in the linear susceptibility. Finally, using the relation between Δ and d given by Equation 6 we find that

$$\Delta = \left(\frac{m\varepsilon_0\alpha}{N^2e^3}\right) \qquad 7.$$

On physical grounds we expect that the linear and nonlinear restoring forces are roughly equal when the displacement x is on the order of the internuclear distance a, or when $\omega_0^2 a \approx \alpha a^2$. In addition, if we make the approximation that $Na^3 \approx 1$ the expression for Δ simplifies to

$$\Delta = a^2/e \qquad 8.$$

For $a = 2$ Å the value for Miller's delta predicted by our simple model is 0.25 m^2/C. This compares very well with the mean value of 0.45 ± 0.07 m^2/C given by Bechmann & Kurtz (95).

Equation 6 shows that the second order susceptibility to a good approximation is given by

$$\begin{aligned} d &= \varepsilon_0\chi(\omega_3)\chi(\omega_2)\chi(\omega_1)\Delta \\ &\approx \varepsilon_0(n^2-1)^3\Delta \approx \varepsilon_0 n^6\Delta \end{aligned}$$

In nonlinear processes d^2/n^3 is the material nonlinear figure of merit. Figure 1 shows this figure of merit and the transparency range for a number of nonlinear materials.

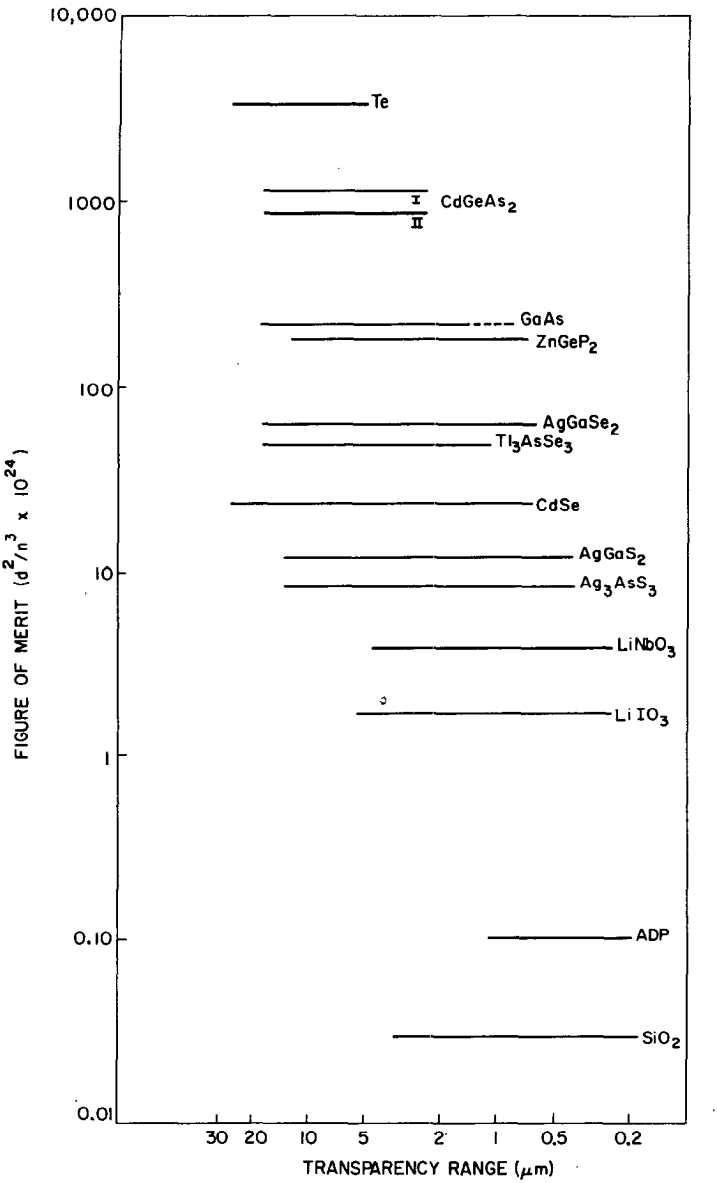

Figure 1 Figure of merit and transparency range for selected nonlinear crystals.

Although d^2/n^3 varies over four orders of magnitude, the intuitive physical picture inherent in the anharmonic oscillator model gives a remarkably accurate account of the magnitude of a material's nonlinear response.

THEORETICAL MODELS Although the anharmonic oscillator model gives insight into the origin of the nonlinear susceptibility, it does not account for the tensor character of $\mathbf{d}$ or allow the calculation of the nonlinear force constant α.

The theory of the nonlinear susceptibility has been the subject of increased consideration. Historically, a quantum treatment based on a perturbation expansion of the susceptibility was the first description put forth for the nonlinear susceptibility (19, 23, 24, 101–104). Unfortunately, in solids, approximations to the quantum result are required to obtain numerical results. In gases, where the wavefunctions are better known, the quantum expressions for the third order susceptibility (second order processes are not allowed by symmetry) do allow predictions of the magnitude of χ^3 which agree very well with measured values (105).

Robinson (106) was the first to attempt to simplify the complete quantum expression for the nonlinear susceptibility. He approached the problem by letting the octapole moment of the ground state charge density serve as the eccentricity of the electronic cloud. Flytzanis & Ducuing (107, 108) and Jha & Bloembergen (109) applied this approach to the III–V compounds.

In the late 1960s Phillips & Van Vechten developed a theory for the dielectric properties of tetrahedrally coordinated compounds (110, 111). This theory, based on Penn's (112) earlier theory of the dielectric susceptibility, is the basis for several models describing the nonlinear susceptibility of crystals (107, 110, 113–119).

Briefly, the theory is based on a single energy gap description of the material which is related to the dielectric constant by

$$\varepsilon(0)-1=\Omega_p^2/E_g^2$$

where $\Omega_p^2=\hbar Ne^2/m\varepsilon_0$ is the plasma energy of the valence (ground state) electrons. Phillips & Van Vechten (110) have shown that the average energy gap E_g can be decomposed into a covalent and ionic part E_h and C by the relation $E_g^2=E_h^2+C^2$, and that the ionicity of the bond is described by $f_i=C^2/E_g^2$. For the ionic or antisymmetric part of the bond, Phillips & Van Vechten (110) have shown that C is described well by

$$C=be^2\left(\frac{Z_A}{r_A}-\frac{Z_B}{r_B}\right)\exp[-k_s(r_A+r_B)/2]$$

where b is a constant, Z_A and Z_B are the valence of elements A and B which form the bond, and k_s is the Thomas-Fermi screening constant.

There are two approaches to calculating the nonlinear susceptibility based on the above theory. The first is to interpret the theory as a two-band model and evaluate the matrix elements appearing in the expansion for the second order susceptibility. This approach has been taken by Flytzanis (107), Phillips & Van Vechten (110),

and Kleinman (116). Using the method, Kleinman shows that the nonlinear coefficient for zincblende compounds is

$$d_{14} = 0.245 \frac{a_0^2}{|e|} \left(\frac{a}{a_0}\right)^{\frac{3}{2}} \frac{C}{E_h} \left(\frac{e^2}{a_0 E_g}\right)^{\frac{1}{2}} \chi^{\frac{3}{2}} \qquad 9.$$

where a_0 is the Bohr radius and χ is the linear susceptibility. The values of d_{14} predicted by Equation 9 are in good agreement with experiment.

The second approach (113, 114) calculates the nonlinear susceptibility from variations in the linear susceptibility under an applied field. In this approach the position of the bond charge can vary (the bond charge model) (113, 120) or a transfer of charge along the bond axis can occur (the charge transfer model) (118, 119). Both approaches give good descriptions of the second order susceptibility. The extension to the third order nonlinear coefficient has been considered recently by Chemla et al (121).

Levine (115) has modified and extended the bond charge model of Phillips & Van Vechten (110). In summary, the bond charge theory does accurately account for both the magnitude and the sign of the nonlinear susceptibility of most nonlinear materials. However, for the purpose of searching for new nonlinear materials or estimating the nonlinear coefficient of a potential nonlinear material, Miller's rule is far simpler to apply.

Second Harmonic Generation

We are now in a position to evaluate the nonlinear interaction in a crystal and to calculate the conversion efficiency and its dependence on phasematching and focusing. Conceptually, it is easier to treat the special case of second harmonic generation and then to extend the principal results to three-frequency interactions.

The starting point for the analysis is Maxwell's equations from which the traveling wave equation is derived in the usual manner. The traveling equation

$$\nabla^2 \mathbf{E} - \mu_0 \sigma \dot{\mathbf{E}} - \mu \varepsilon \ddot{\mathbf{E}} = \mu_0 \ddot{\mathbf{P}} \qquad 10.$$

describes the electric field in the medium with a linear dielectric constant ε driven by the nonlinear driving polarization $\partial^2 \mathbf{P}/\partial t^2$. It is customary to define the fields by the Fourier relations

$$\mathbf{E}(\mathbf{r}, t) = \tfrac{1}{2}[\mathbf{E}(\mathbf{r}, \omega) \exp\{i(\mathbf{k} \cdot \mathbf{r} - \omega t)\} + c.c.]$$

and

$$\mathbf{P}(\mathbf{r}, t) = \tfrac{1}{2}[\mathbf{P}(\mathbf{r}, \omega) \exp\{i(\mathbf{k} \cdot \mathbf{r} - \omega t)\} + c.c.]$$

Substituting into Equation 10 making the usual slowly varying amplitude approximations that $\omega^2 \mathbf{P} \gg \omega \dot{\mathbf{P}} \gg \ddot{\mathbf{P}}$, $\mathbf{k}\, \partial E/\partial z \gg \partial^2 \mathbf{E}/\partial z^2$, and $\omega \mathbf{E} \gg \dot{\mathbf{E}}$, and letting $\alpha = \frac{1}{2}\mu\sigma c$ be the electric field loss per length, gives

$$\frac{\partial \mathbf{E}}{\partial z} + \alpha \mathbf{E} + \frac{1}{c} \frac{\partial \mathbf{E}}{\partial t} = \frac{i \mu_0 c \omega \mathbf{P}}{2}$$

for the equation relating the envelope quantities of the fields. Neglecting loss,

assuming a steady state solution, and using the definition given by Equation 3 for the driving polarization, the above equation reduces to a pair of coupled nonlinear equations for the fundamental and second harmonic waves

$$\frac{d\mathbf{E}(\omega)}{dz} = i\kappa \mathbf{E}(2\omega)\mathbf{E}^*(\omega)\exp(i\Delta\mathbf{k}z) \qquad 11a.$$

$$\frac{d\mathbf{E}(2\omega)}{dz} = i\kappa \mathbf{E}(\omega)\mathbf{E}(\omega)\exp(-i\Delta\mathbf{k}z) \qquad 11b.$$

where $\kappa = \omega d/nc$ and $\Delta\mathbf{k} = \mathbf{k}(2\omega) - 2\mathbf{k}(\omega)$ is the wavevector mismatch. At phase-matching $\Delta\mathbf{k} = 0$ and $n(\omega) = n(2\omega)$ since $\mathbf{k} = 2\pi n/\lambda$ where n is the index of refraction. Here we have introduced the interaction constant κ which includes the nonlinear coefficient d.

The above coupled equations for second harmonic generation have been solved exactly (19). It is useful to discuss the solution for second harmonic generation since the results can be extended to three-frequency interactions. We proceed by considering the low conversion efficiency case for a nonzero $\Delta\mathbf{k}$, and then the high conversion efficiency case.

In the low conversion limit, the fundamental wave is constant with distance. Therefore, we set $d\mathbf{E}(\omega)/d\mathbf{z} = 0$ and integrate Equation 11b

$$\int_0^{\mathbf{E}(z=l)} d\mathbf{E}(2\omega) = \int_{-l/2}^{l/2} i\kappa \mathbf{E}^2(\omega)\exp(-i\Delta\mathbf{k}z)\,dz$$

which gives

$$\mathbf{E}(2\omega)\big|_{z=l} = i\kappa \mathbf{E}^2(\omega)\frac{[\exp(i\Delta\mathbf{k}l/2) - \exp(i\Delta\mathbf{k}l/2)]}{i\Delta\mathbf{k}}$$

$$= \kappa \mathbf{E}^2(\omega) l \frac{\sin(\Delta\mathbf{k}l/2)}{(\Delta\mathbf{k}l/2)}$$

If we denote $(\sin x)/x$ by $\operatorname{sinc} x$, note that the intensity is given by

$$I = \frac{nc\varepsilon_0}{2}|\mathbf{E}|^2$$

then in the low conversion limit, the conversion efficiency is

$$\frac{I(2\omega)}{I(\omega)} = \Gamma^2 l^2 \operatorname{sinc}^2\left(\frac{\Delta\mathbf{k}l}{2}\right) \qquad 12.$$

where

$$\Gamma^2 l^2 = \kappa\kappa |\mathbf{E}(\omega)|^2 l^2$$

$$= \frac{2\omega^2 |d|^2 l^2 I(\omega)}{n^3 c^3 \varepsilon_0} \qquad 13.$$

This example shows that phasematching enters into the nonlinear conversion process through the phase synchronism factor $\operatorname{sinc}^2(\Delta kl/2)$ which is unity at $\Delta kl = 0$.

Also, the second harmonic conversion efficiency is proportional to $|d|^2$ and l^2, as expected, and varies as the fundamental intensity. The above result holds in the plane wave focusing limit where $I = P/A$ and the area $A = \pi w_0^2/2$ with w_0 the gaussian beam electric field radius.

For high conversion efficiencies, Equations 11a and 11b can be solved by invoking energy conservation such that $\mathbf{E}^2(\omega)+\mathbf{E}^2(2\omega) = \mathbf{E}_{\text{inc}}^2$ where $\mathbf{E}_{\text{inc}}$ is the incident electric field at $z = 0$. The solution for perfect phasematching is the well known result

$$\frac{I(2\omega)}{I(\omega)} = \tanh^2(\kappa \mathbf{E}_{\text{inc}} z)$$

which for small $\kappa \mathbf{E}_{\text{inc}} z$ reduces to the low conversion efficiency result. In theory, second harmonic generation should approach 100% as a $\tanh^2 x$ function. In practice, conversion efficiencies of 40–50% are reached under optimum focusing conditions.

The solutions for second harmonic generation suggest that phasematching and focusing are important if maximum conversion efficiency is to be achieved. The important aspects of phasematching and focusing are discussed next.

PHASEMATCHING It immediately follows from Equation 12 that for second harmonic generation to be efficient, $\Delta\mathbf{k}$ must be zero. As stated earlier, this is accomplished in birefringent crystals by utilizing the birefringence to overcome the crystal dispersion between the fundamental and second harmonic waves. As a specific example, consider phasematching in the negative ($n_e < n_0$) uniaxial crystal KDP.

For a beam propagating at an angle θ_m to the crystal optic axis, the extraordinary index is given by

$$\left[\frac{1}{n_e(\theta_m)}\right]^2 = \frac{\cos^2\theta_m}{n_0^2} + \frac{\sin^2\theta_m}{n_e^2}$$

where n_0 and n_e are the ordinary and extraordinary indices of refraction at the wavelength of interest. Two types of phasematching are possible for negative uniaxial KDP:

$$\text{Type I} \quad n_e^{2\omega}(\theta_m) = n_o^{\omega}$$

$$\text{Type II} \quad n_e^{2\omega}(\theta_m) = \tfrac{1}{2}[n_e^{\omega}(\theta_m)+n_o^{\omega}]$$

For positive uniaxial crystals ($n_e > n_o$) the extraordinary and ordinary indices are reversed in the Type I and II phasematching expressions (35).

Type I phasematching uses the full birefringence to offset dispersion and Type II phasematching averages the birefringence to use effectively half of it in offsetting the dispersion. A more important factor in choosing the type of phasematching to be used is the nonlinear coefficient tensor. It must be evaluated to see that the effective nonlinear coefficient remains nonzero. Thus for KDP where the $\bar{4}2m$ nonlinear tensor has components given by Equation 3, Type I phasematching requires that the second harmonic wave be extraordinary or polarized along the crystallographic z axis. To generate this polarization, the fundamental waves must be

polarized in the $\mathbf{E}_x$ and $\mathbf{E}_y$ direction and thus be ordinary waves. In addition, the product $\mathbf{E}_x\mathbf{E}_y$ should be maximized. Therefore, the propagation direction in the crystal should be in the (110) plane at θ_m to the crystal optic or z axis. For this case, the effective nonlinear coefficient becomes $d_{\text{eff}} = d \sin\theta_m$ and it is this coefficient that is used in the SHG conversion efficiency expression. The effective nonlinear coefficients for other crystal point groups have been calculated and listed (37, 97). In addition, the phasematching angles for a number of nonlinear crystals and pump lasers have been listed by Kurtz (122).

The above discussion for uniaxial crystals can be extended to biaxial crystals. As one might expect, the generalization becomes complicated. However, Hobden (123) has given a complete description of the process including a careful definition of the three principle indices n_α, n_β, and n_γ.

One other aspect of phasematching is important in limiting SHG conversion efficiency. As the extraordinary wave propagates in the crystal, its power flow direction differs by the double refraction angle ρ from its phase velocity direction. This walk-off of energy at the doubled refraction angle leads to a decrease in SHG efficiency due to the separation of the ordinary fundamental wave and the extraordinary second harmonic wave. The double refraction angle is given by

$$\rho \approx \tan\rho = \frac{n_o^2(\omega)}{2}\left[\frac{1}{n_e^2(2\omega)} - \frac{1}{n_o^2(2\omega)}\right]\sin 2\theta_m$$

Note that $\rho = 0$ at $\theta = 0$ and $\theta = \pi/2$. The latter angle corresponds to a propagation direction 90° to the crystal optic axis. Phasematching in this direction is referred to a 90° phasematching and has the advantage of not inducing Poynting vector walk-off. As shown in the next section, when $\rho \neq 0$, the effective interaction length in the crystal may be considerably reduced, thus reducing the conversion efficiency. Therefore, 90° phasematching is desirable when possible.

FOCUSING Up to this point we have assumed that the interacting waves are plane waves of infinite extent. In fact, the beams are usually focused into the nonlinear crystal to maximize the intensity and interaction length. In addition, the waves are usually generated by laser sources and thus have a Gaussian amplitude profile with electric field radius w. Gaussian beam propagation theory and laser resonators have been treated by a number of authors and will not be considered here. For the present discussion, the important factors of interest are (*a*) the form of the Gaussian beam

$$\mathbf{E} = \mathbf{E}_0 \exp(-\mathbf{r}^2/w^2)$$

(*b*) the relation between the peak power and intensity

$$P = I \cdot A = I\left(\frac{\pi w^2}{2}\right)$$

and (*c*) twice the distance over which the beam area doubles

$$b = \mathbf{k}w^2 = \frac{2\pi n}{\lambda}w^2 \qquad 14.$$

which is called the confocal distance.

To include focusing, the SHG efficiency can be written in the form

$$\frac{I(2\omega)}{I(\omega)} = \left(\frac{2\omega^2 d_{\text{eff}}^2}{\pi n_\omega n_{2\omega} \varepsilon_0 c^3}\right) P_\omega l \mathbf{k}_\omega h(B, \xi) \qquad 15.$$

where l is the crystal length, $\mathbf{k}_\omega$ the wavevector in the crystal at the fundamental frequency, and $h(B, \xi)$ is the Boyd & Kleinman (97) focusing factor. The focusing factor $h(B, \xi)$ is a function of the double refraction parameter

$$B = \tfrac{1}{2}\rho(l\mathbf{k}_\omega)^{\frac{1}{2}}$$

and the focusing parameter

$$\xi = l/b$$

where b is the confocal distance given by Equation 14.

In general, $h(B, \xi)$ is an integral expression involving B and ξ. However, it reduces to simplified expressions in the proper limits. If we introduce the aperture length l_a given by

$$l_a = \frac{w\sqrt{\pi}}{\rho}$$

and an effective focal length l_f given by

$$l_f = \frac{\pi w^2 k}{2} = \frac{2}{\pi} b$$

then the second harmonic conversion efficiency takes the limiting forms

$$\frac{I(2\omega)}{I(\omega)} = \frac{KP_\omega}{w^2} \cdot \begin{cases} l^2 & \text{for } (l_a, l_f \gg l) \\ l l_a & \text{for } (l_f \gg l \gg l_a) \\ l_f l_a & \text{for } (l \gg l_f \gg l_a) \\ 4l_f^2 & \text{for } (l \gg l_a \gg l_f) \\ 4.75 l_f^2 & \text{for } (l_a \gg l \gg l_f) \end{cases}$$

The first limit corresponds to the plane wave focusing case where $h(\xi, B) \approx l/b$. This case holds until $l/b \approx 1$, which is called the confocal focusing limit. The second harmonic conversion efficient is optimum at $l/b = 2.84$ where $h(2.84, 0) = 1.06$ (97).

If $\rho \neq 0$, then the aperture length may limit the interaction length to the second and third cases. In practice, even a small walk-off angle may reduce the second harmonic efficiency by 30 times for a given crystal length and focusing. It is therefore very desirable to adjust the crystal indices of refraction to achieve 90° phase-matching if possible. In general, the last three of the above limits are not encountered experimentally. This discussion on focusing is intended to serve as a general introduction. A more detailed presentation is given by Boyd & Kleinman (97).

Three-Frequency Interactions

Three-frequency interactions include sum generation and difference frequency generation or mixing in which two waves are incident on the nonlinear crystal and

interact to generate a third wave, and parametric generation in which a high power pump frequency interacts in a nonlinear crystal to generate two tunable frequencies.

We denote the three frequencies by ω_1, ω_2, and ω_3 such that $\omega_3 = \omega_2 + \omega_1$ is the energy conservation condition and $\mathbf{k}_3 = \mathbf{k}_2 + \mathbf{k}_1 + \Delta\mathbf{k}$ is the momentum conservation condition with $\Delta\mathbf{k}$ the momentum mismatch.

If we consider $LiNbO_3$ as an example, the generated polarization now has three components given by

$$\mathbf{P}(\omega_1) = \varepsilon_0 2d_{31}\mathbf{E}(\omega_3)\mathbf{E}^*(\omega_2)$$
$$\mathbf{P}(\omega_2) = \varepsilon_0 2d_{31}\mathbf{E}(\omega_3)\mathbf{E}^*(\omega_1)$$
$$\mathbf{P}(\omega_3) = \varepsilon_0 2d_{31}\mathbf{E}(\omega_2)\mathbf{E}(\omega_1)$$

Substituting the polarization and electric field expressions at ω_1, ω_2, and ω_3 into the wave equation given by Equation 10 gives three coupled equations similar to the two coupled equations previously derived for the SHG case:

$$\frac{d\mathbf{E}_1}{dz} + \alpha_1\mathbf{E}_1 = \kappa_1\mathbf{E}_3\mathbf{E}_2^* \exp(i\Delta\mathbf{k}z) \qquad 16a.$$

$$\frac{d\mathbf{E}_2}{dz} + \alpha_2\mathbf{E}_2 = i\kappa_2\mathbf{E}_3\mathbf{E}_1^* \exp(i\Delta\mathbf{k}z) \qquad 16b.$$

$$\frac{d\mathbf{E}_3}{dz} + \alpha_3\mathbf{E}_3 = i\kappa_3\mathbf{E}_1\mathbf{E}_2 \exp(-i\Delta\mathbf{k}z) \qquad 16c.$$

where $\mathbf{E}(\omega_1)$ is now written $\mathbf{E}_1$, $\kappa_i = \omega_i d/n_i c$, and α_i is the loss.

We next investigate the solution of the above coupled equations for the three frequency processes of interest. The coupled equations have been solved exactly (19, 124); however, we consider only the simplified case of interacting plane waves and weak interactions such that the pump wave is not depleted.

SUM GENERATION (UP-CONVERSION) For the case of sum generation ω_1 is a weak infrared wave that sums with a strong pump wave at ω_2 to generate a high frequency (visible) wave at ω_3. Negligible pump depletion implies that $d\mathbf{E}_2/dz = 0$ so that the three coupled equations reduce to a pair of Equations (16a and 16c). If we assume no loss, $\Delta\mathbf{k} = 0$, and a solution of the form $e^{\Gamma z}$ with input boundary conditions that $\mathbf{E}_3(z=0) = 0$ and $\mathbf{E}_1(z=0) = \mathbf{E}_1(0)$, the solution of the coupled equations is

$$\mathbf{E}_1(z) = \mathbf{E}_1(0)\cos\Gamma z$$

$$\mathbf{E}_3(z) = \sqrt{\frac{\omega_3}{\omega_1}}\mathbf{E}_1(0)\sin\Gamma z$$

where

$$\Gamma = \sqrt{\kappa_1\kappa_2|\mathbf{E}_2|^2}$$

Thus sum generation has an oscillatory solution with no net gain and a 100% conversion for $\Gamma z = \pi/2$. In the low conversion limit, $\sin\Gamma z \approx \Gamma z$ so that the up-conversion efficiency becomes

$$\frac{I_3}{I_1(0)} = \left(\frac{\omega_3}{\omega_1}\right)\Gamma^2 l^2 \operatorname{sinc}^2\left(\frac{\Delta \mathbf{k} l}{2}\right) \qquad 17.$$

where $\Gamma^2 l^2 = (2\omega_1\omega_3 d^2 l^2 I_2)/(n_1 n_2 n_3 c^3 \varepsilon_0)$ is equal to the previously derived SHG conversion efficiency factor given by Equation 13. In the low conversion efficiency limit the sum generation efficiency equals the SHG efficiency as one expects from physical arguments. However, at high conversion efficiencies the sum generation conversion oscillates while the SHG conversion approaches 100% as $\tanh^2 \Gamma z$.

Sum generation has been used to generate new frequencies in the same way as SHG. For example, 10.6 μm has been summed with 5.3 μm in $CdGeAs_2$ (125) to generate the third harmonic of 10.6 μ at 3.5 μm. Similar summing has been used to generate the third harmonic frequency of a 1.06 μm Nd:YAG laser in KDP with 60% efficiency (126).

Sum generation also allows infrared waves to be up-converted to the visible for detection by a photomultiplier. Infrared up-conversion has been extensively studied (127–129) and applied to astronomical uses (47).

DIFFERENCE FREQUENCY GENERATION. For difference frequency generation or mixing the pump is the high frequency field at ω_3. Therefore, lack of pump depletion implies $d\mathbf{E}_3/dz = 0$ so that the coupled equations reduce to Equations 16a and 16b. Again assuming a solution of the form $e^{\Gamma z}$ and boundary conditions that $\mathbf{E}_1(z=0) = \mathbf{E}_1(0)$ and $\mathbf{E}_2(0) = 0$ results in the solution

$$\mathbf{E}_1(z) = \mathbf{E}_1(0)\cosh \Gamma z$$

$$\mathbf{E}_2^*(z) = \sqrt{\frac{\omega_2}{\omega_1}}\,\mathbf{E}_1(0)\sinh \Gamma z$$

Now we notice that exponential functions have replaced the sin and cos functions which occurred in the sum generation case. This implies that both the input field at ω_1 and the generated difference field at ω_2 grow during the nonlinear interaction at the expense of the pump field. Again in the limit of low conversion efficiency where $\sinh \Gamma l \approx \Gamma l$ the mixing efficiency becomes

$$\frac{I_2}{I_1(0)} = \left(\frac{\omega_2}{\omega_1}\right)\Gamma^2 l^2 \operatorname{sinc}^2\left(\frac{\Delta \mathbf{k} l}{2}\right) \qquad 18.$$

where $\Gamma^2 l^2 = (2\omega_1\omega_2 d^2 l^2 I_3)/(n_1 n_2 n_3 c^3 \varepsilon_0)$ is the conversion efficiency which equals the SHG and sum generation efficiency. However, now both waves grow and have net gain. This suggests the possibility of parametric oscillation once the gain exceeds the losses.

Difference frequency generation or mixing has been used to measure parametric gain (130) and to generate new frequencies. Of particular interest is the generation of infrared and far infrared radiation by mixing in nonlinear crystals. A number of experiments have recently been carried out using visible dye laser sources (56, 57) and near infrared sources (59, 61) to generate tunable infrared output.

PARAMETRIC GENERATION For this case we assume a strong pump wave at ω_3 and equal input fields at ω_1 and ω_2. Again the three coupled equations reduce to

Equations 16a and 16b in the absence of pump depletion. The remaining pair of equations are the same as for mixing; however, now the boundary conditions that $\mathbf{E}_1(z=0) = \mathbf{E}_1(0)$ and $\mathbf{E}_2(z=0) = \mathbf{E}_2(0)$ are inputs into the system. In fact, the input fields need be only the quantum noise field associated with the gain of the parametric amplifier.

The general solution of Equations 16a and 16b for the above boundary conditions has been given by Harris (79) and by Byer (85) in their review articles on parametric oscillators and is too long to reproduce here. However, for a single frequency incident on a parametric amplifier, the gain defined by $G_2(l) = (|\mathbf{E}_2(l)|^2/|\mathbf{E}_2(0)|^2) - 1$ simplifies to

$$G_2(l) = \Gamma^2 l^2 \frac{\sinh^2 gl}{gl} \qquad 19.$$

where $\Gamma^2 l^2 = (2\omega_1\omega_2 d^2 l^2 I_3)/(n_1 n_2 n_3 c^3 \varepsilon_0)$ and $g = [\Gamma^2 - (\Delta\mathbf{k}/2)^2]^{\frac{1}{2}}$. In the low gain limit Equation 19 reduces to

$$G_2(l) = \Gamma^2 l^2 \operatorname{sinc}^2\left(\frac{\Delta\mathbf{k}l}{2}\right) \qquad 20.$$

which shows that the parametric gain equals the SHG conversion efficiency in this limit. In the high gain limit Equation 19 reduces to

$$G_2(l) = (1/4)\exp(2\Gamma l) \qquad 21.$$

for $\Delta\mathbf{k}/2 \ll g$. In practice high gains have been reported (65, 86, 131) such that superradiant operation is possible (126, 132).

Parametric amplifiers, like all linear amplifiers, have inherent noise. Since the parametric frequencies can be in the visible range and are on the order of 10^{-10} W per watt of pump power, the noise emission is intense enough to be easily visible as parametric fluorescence (133, 134). A striking color photograph of parametric fluorescence generated in $LiNbO_3$ (135) is reproduced in a review article by Giordmaine (136). Parametric noise emission can be considered generated by the amplified zero point fluctuations of the electromagnetic field (137–139). It can be shown that the fluorescence noise power is given simply by P_{noise} = (energy per photon) × gain × bandwidth or approximately by $P_{\text{noise}} = \hbar\omega \times \Gamma^2 l^2 \times (c/2\Delta n l)$ where Δn is the crystal birefringence and l the crystal length. For $LiNbO_3$ the emitted noise power per watt is approximately 10^{-10} W, or one order of magnitude larger than the spontaneous Raman scattering power. The noise power can be used to measure the gain, bandwidth, and tuning characteristics of a parameter oscillator prior to ever achieving threshold (133, 134). Parametric fluorescence also provides a very accurate method of measuring the nonlinear coefficient of a crystal since only a power ratio need be measured and not an absolute power as for SHG measurements (137). However, one of the most interesting applications of parametric generation is the achievement of coherent tunable laser-like output from an optical parametric oscillator.

Parametric Oscillators

A parametric oscillator is schematically represented by a nonlinear crystal within an optical cavity. The nonlinear crystal when pumped provides gain at the two

frequencies ω_2 and ω_1 (the signal and idler fields). When the gain exceeds the loss the device reaches threshold and oscillates. At threshold the output power increases dramatically, similar to the behavior of a laser. The generated output is coherent and collinear with the pump laser beam. Once above threshold, the parametric oscillator efficiently converts the pump radiation to continuously tunable signal and idler frequencies.

There are a number of configurations for an optical parametric oscillator (OPO). The first distinction is between cw and pulsed operation. Due to the much higher gains, we consider only pulsed operation where the pump is typically generated by a Q-switched laser source. Parametric oscillators have also operated internal to the pump laser cavity, but the external configuration is more common. Finally, there are different parametric oscillator cavity configurations. The two most important are the doubly resonant oscillator (DRO), where both the signal and idler waves are resonated by the cavity mirrors, and the singly resonant oscillator (SRO), where only one wave is resonant. The operation characteristics of parametric oscillators with these cavity configurations have been discussed in detail in the review articles by Harris (79), Smith (84), and Byer (85).

The important differences between DRO and SRO operation include threshold, frequency stability, and pump laser frequency requirements. The threshold of a DRO occurs when the gain equals the product of the signal and idler losses or

$$\Gamma^2 l^2 \operatorname{sinc}^2\left(\frac{\Delta \mathbf{k} l}{2}\right) = a_1 a_2 \qquad 22.$$

where $\Gamma^2 l^2$ given by Equation 19 is the single pass parametric gain and a_2, a_1 are the single pass power losses at the signal and idler. The SRO threshold is greater than that of the DRO. If the idler wave at ω_1 is not resonated, then the SRO threshold becomes

$$\Gamma^2 l^2 \operatorname{sinc}^2\left(\frac{\Delta \mathbf{k} l}{2}\right) = 2a_2 \qquad 23.$$

which is $2/a_1$ times greater than the DRO threshold. As an example consider a 5 cm long 90° phasematched $LiNbO_3$ crystal pumped by the second harmonic of a Nd:YAG laser at 0.532 μm. The DRO pump power threshold for 2% losses at ω_1 and ω_2 is only 38 mW. The SRO threshold is increased to 3.8 W. For cw pump lasers the DRO is required in order to achieve threshold. However, for pulsed parametric oscillator operation where kilowatts of pump power is available, the higher SRO threshold is not a disadvantage and singly resonant offers significant advantages over doubly resonant operation.

One obvious advantage of the SRO is the much simpler mirror coating requirement since only one wave is resonated. The DRO also requires a single frequency pump wave (79), whereas the SRO can be pumped by a multiple axial mode source which more closely approximates typical laser characteristics. Finally, the DRO operates with large frequency fluctuations since the condition $\omega_p = \omega_s + \omega_1$ must hold for each parametric oscillator cavity mode and pump frequency. This leads to mode jumping and the so-called "cluster effect" (67) in output frequencies where

only a cluster of a few adjacent axial modes oscillate within the gain linewidth of the parametric oscillator. Since the SRO has only a single cavity none of these frequency competition effects occur. In fact, the SRO can be pumped with a multiple axial mode pump laser source and still operate at a single frequency for the resonated wave. These factors make singly resonant operation desirable whenever possible.

The conversion efficiency of parametric oscillators has been studied in detail and is discussed in the previously mentioned review papers. Briefly, the DRO theoretically should be 50% efficient and the SRO near 100% efficient. In practice the DRO efficiency approaches 50% and the SRO efficiency is near 40% although 60–70% conversion efficiencies have been obtained.

The tuning and bandwidth of a parametric oscillator are determined by the phasematching condition $\mathbf{k}_3 = \mathbf{k}_2 + \mathbf{k}_1$ and the sinc $(\Delta \mathbf{k} l/2)$ phase synchronism factor.

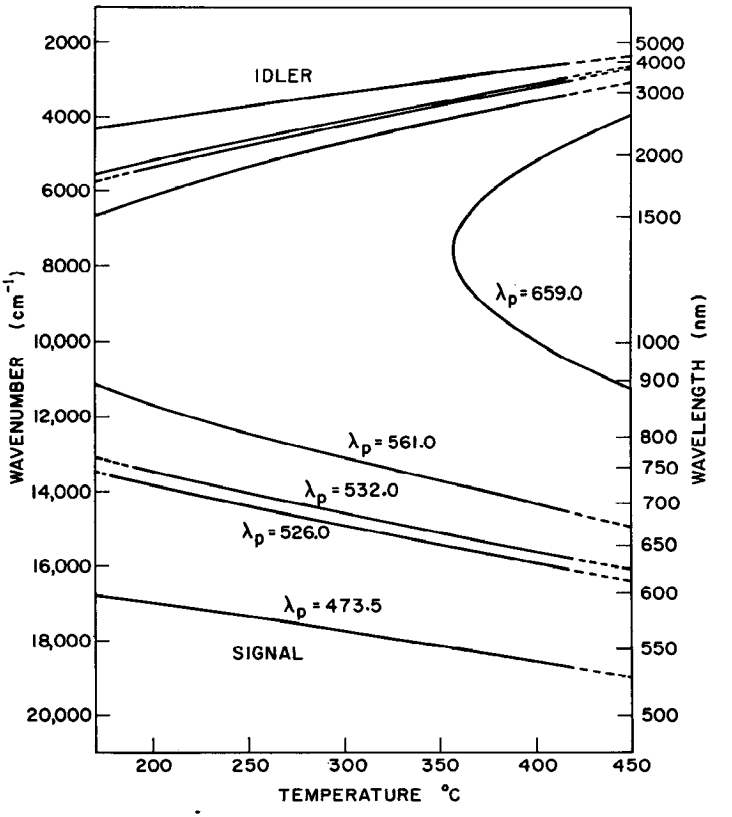

Figure 2 $LiNbO_3$ parametric oscillator tuning curves for various doubled Nd:YAG laser pump wavelengths.

In general, a parametric oscillator is tuned by altering the crystal birefringence. This is usually done by crystal rotation, thus changing the extraordinary index of refraction, or by controlling the crystal temperature and thus the birefringence. As an example Figure 2 shows the temperature tuning curves of a $LiNbO_3$ parametric oscillator pumped by various doubled wavelengths of a Q-switched Nd:YAG laser. The tuning range extends from 0.55 to 3.7 μm. Tuning curves for a number of nonlinear crystals have been given in the review article by Byer (85).

The gain bandwidth of a parametric oscillator is found by analyzing the $\text{sinc}^2(\Delta\mathbf{k}l/2)$ function. Letting $\Delta\mathbf{k}l/2 = \pi$ define the bandwidth gives

$$\delta\omega = 2\pi/\beta l$$

where

$$\beta = [(\partial\mathbf{k}_1/\partial\omega_1) - (\partial\mathbf{k}_2/\partial\omega_2)]$$

is the crystal dispersion factor. Expanding β in terms of the crystal index of refraction shows that $\beta \approx 2\Delta n/c$ so that the parametric oscillator gain bandwidth in wavenumbers is approximately

$$|\delta\nu(\text{cm}^{-1})| = \frac{1}{2\Delta n l} \qquad 24.$$

where Δn is the birefringence and l the crystal length. A 5 cm long $LiNbO_3$ parametric oscillator has approximately a 1 cm^{-1} gain bandwidth.

Like laser sources, the parametric oscillator can oscillate over a narrower frequency range than the full gain bandwidth. In this regard, the parametric oscillator acts like a homogeneously saturated laser and can operate in a single axial mode without a reduction of the conversion efficiency. Linewidths as narrow as 0.001 cm^{-1} or 30 MHz have been achieved with $LiNbO_3$ parametric oscillators (for further discussion see Byer, 85).

More than any other device the optical parametric oscillator requires a uniform high optical quality, low loss nonlinear crystal. In addition, the crystal must have adequate birefringence to phasematch and be able to withstand the high laser intensities needed to reach threshold without damaging. These linear and nonlinear optical material requirements are discussed in detail in the following section.

NONLINEAR MATERIALS

Material Requirements

Nonlinear crystals must satisfy four criteria if they are to be useful for nonlinear optical applications. These criteria are adequate nonlinearity and optical transparency, proper birefringence for phasematching, and sufficient resistance to optical damage by intense optical irradiation. These properties are briefly discussed in the next four sections. They are then illustrated by descriptions of useful nonlinear crystals.

NONLINEARITY In the early days of nonlinear optics adequate laser power was not always available to take full advantage of the potential conversion efficiency of a

nonlinear crystal. Under those circumstances, the highest crystal nonlinearity was a very important factor. Since the late 1960s the situation has changed chiefly due to the availability of well controlled high peak power laser sources at many wavelengths across the ultraviolet, visible, and infrared spectral regions. Under present circumstances, the crystal nonlinearity becomes only one factor in determining the crystal's potential for nonlinear applications. For example, if more than adequate laser power is available, then the nonlinear conversion efficiency is determined by the maximum incident intensity the crystal can withstand without damaging. In addition, the nonlinear conversion efficiency is then more usefully expressed at a given intensity rather than power level. Finally, in comparing nonlinear crystals with more than five orders of magnitude range in their figures of merit as illustrated by Figure 1, one finds that most crystals have very nearly the same conversion efficiency at a fixed intensity. This remarkable fact is illustrated by Figure 3 which

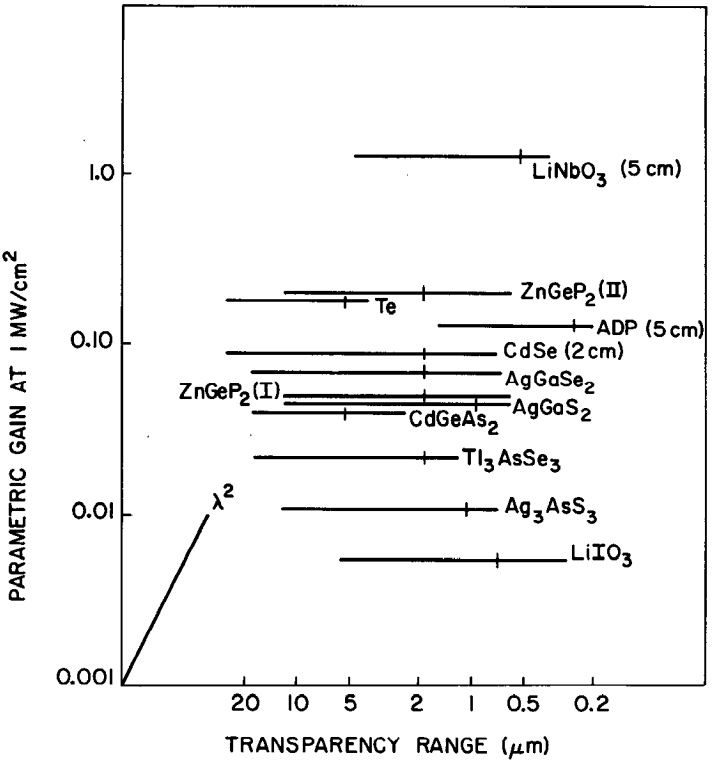

Figure 3 Nonlinear conversion efficiency (parametric gain) at 1 MW/cm^2 pump intensity and transparency range of nonlinear crystals. The pump wavelength for parametric conversion (second harmonic wavelength for SHG) is shown by the vertical tick mark. The nonlinear efficiency varies as the square of the pump wavelength and crystal length. The crystal lengths are taken to be 1 cm unless specified.

shows the parametric gain for a number of nonlinear materials. Under the present circumstances, the magnitude of a crystal's nonlinear coefficient is not of paramount importance, but must be taken into account along with the other material parameters.

The measurement of crystal nonlinear coefficients has continued at a rapid pace so that there are extended tables available listing nonlinear coefficients (35, 85, 95, 122). The measurement of absolute nonlinear coefficients has been carried out by a number of methods including second harmonic generation (140, 141), mixing (58), and parametric fluorescence (137). The latter method has the advantage of being a relative power measurement and not requiring the absolute measurement of power as for SHG. Relative nonlinear coefficient measurements have also been made by three methods: the powder technique (142), the Maker fringe method (4, 143), and the wedge technique (144–146). The latter method is particularly useful in that it gives, in addition to the relative magnitude of the nonlinear coefficient, the relative sign and the coherence length of the interaction. At this time, absolute nonlinear coefficients have been measured for a number of crystals including ADP, KDP, $LiIO_3$, $LiNbO_3$, Ag_3SbS_3, CdSe, and $AgGaSe_2$. In the visible $LiIO_3$ and KDP and in the infrared GaAs are used as standard nonlinear crystals. There is interest in improving the accuracy of measurement for nonlinear coefficients and work is in progress toward that goal.

TRANSPARENCY Known nonlinear materials have transparency ranges that extend from 2200 Å in ADP through the infrared in a number of semiconductor compounds and beyond the reststrahl band into the far infrared in both oxide and semiconductor crystals. In general, the transparency range in a single material is limited by the band edge absorption at high frequencies and by two-phonon absorption at twice the reststrahlen frequency at low frequencies. Materials are also transparent in the very low frequency range between dc and the first crystal vibrational mode. Thus nonlinear interactions may extend from the ultraviolet through the visible and infrared to the far infrared. In fact, only a few crystals having the proper birefringence and overlapping transparency ranges are needed to cover the entire extended frequency range. This is important because the growth of high optical quality nonlinear crystals is, in general, a difficult task. In addition, nonlinear crystals that can be grown well, are transparent, and have proper birefringence for phasematching are very rare among all known acentric crystals (147). For example, among 13,000 surveyed crystals only 684, or 5.25%, are uniaxial and phasematchable, and of these less than half have a nonlinearity greater than KDP and far fewer are amenable to crystal growth in high optical quality centimeter sizes.

The transmission loss in a nonlinear crystal reduces the SHG conversion efficiency by $e^{-(\alpha_2/2+\alpha_1)l}$ where α_2 and α_1 are the loss per length at the second harmonic and fundamental waves. Thus a 0.05 cm^{-1} and 0.025 cm^{-1} loss at 2ω and ω in a 1 cm long crystal reduces the SHG efficiency by 0.95, which is negligible. However, in a 5 cm crystal the same losses reduce the efficiency by a factor of 0.77, which is significant. High optical quality oxide materials have losses in the 10^{-3} to 10^{-5} cm^{-1} range, whereas semiconductor materials show much higher losses in the 1 cm^{-1} to 10^{-2} cm^{-1} range. The reduction of optical loss in nonlinear

crystals is important if the nonlinear interaction is to proceed efficiently. It becomes even more important for operation of a parametric oscillator where the threshold pumping power and operating efficiency directly depend on the crystal and cavity losses.

Recently intensity-dependent losses have been recognized as important factors in the transparency of a crystal. At the short wavelength end of a material's transparency range, two-photon absorption may become the dominant loss mechanism even in a frequency range that is normally transparent to low intensity radiation. For example, at 10 MW/cm^2 the two-photon absorption in GaAs at 1.32 μm is 0.3 cm^{-1}, which is significant compared to the 0.05 cm^{-1} normal absorption loss (148). This nonlinear absorption mechanism has also been observed in oxide nonlinear materials for intense pump radiation within the two-photon frequency range of the band edge. Thus for maximum efficiency, pump wavelengths must be longer than the two-photon absorption edge of the nonlinear crystal, although operation near the band edge is possible at lower efficiencies and pump intensities. Gandrud & Abrams (45) have reported an additional loss mechanism in tellurium due to two-photon induced free carrier absorption. This mechanism reduced the SHG conversion efficiency from 15 to 5% for doubling a CO_2 laser source.

The two-photon absorption limit was in mind when pump wavelengths for the parametric gain calculations shown in Figure 3 were chosen. Figure 3 does illustrate that with a few nonlinear materials, nonlinear interactions are possible over the entire 2200 Å to 30 μm spectral region. Thus there is the possibility of generating continuously tunable coherent radiation in nonlinear crystals over this extended spectral range.

BIREFRINGENCE AND PHASEMATCHING For efficient nonlinear interactions phasematching must be achieved in the nonlinear crystal. As an example, SHG in cubic crystals that lack birefringence and thus are not phasematchable occurs only over a distance of one coherence length between 10–100 μm. By using birefringence to offset dispersion, the phasematched interaction may proceed over the full crystal length, or approximately 1 cm. Since the SHG efficiency varies as l^2, phasematching increases the efficiency by at least 10^4. The enormous improvement in nonlinear conversion efficiency due to phasematching makes phasematching essential in nonlinear crystals. Thus if a crystal is nonlinear and transparent, it must still phasematch to be useful. Adequate birefringence for phasematching is the most restrictive requirement placed on a crystal and reduces the number of potential crystals to only a few hundred out of over 13,000 known crystals.

In conducting surveys for new nonlinear crystals, the crystal symmetry is determined by X-ray methods or by reference to existing tables (149). If the crystal is acentric and belongs to a point group that gives nonzero nonlinear coefficients for phasematching (see Kurtz, 122, for further discussion) then the crystal indices of refraction and birefringence must be determined. Fortunately, mineralogy texts and data collections are available (150) which list indices of refraction and birefringence for a large number of crystals. A comparison of the crystal birefringence against its index of refraction and similar quantities for known phasematchable crystals gives

a quick indication of whether the potential nonlinear crystal has adequate birefringence for phasematching. Wemple (151), Wemple & DiDomenico (152), and Byer (147) have plotted birefringence vs index of refraction for known nonlinear crystals to determine the minimum required birefringence for phasematching. Such plots are useful since birefringence of a particular crystal cannot accurately be determined theoretically at this time.

Of course the above preliminary indications of possible phasematching in a new material must be carried a step further to determine the actual phasematching properties of a crystal. This is usually done by accurately measuring the crystal indices of refraction and fitting the results to an analytical expression which is useful for phasematching calculations. The measurement of crystal indices of refraction is tedious experimentally, especially in the infrared, so that complete measurements have been made on only a few crystals (35, 95). The measurements must be accurate to 0.01% for phasematching calculations to be made. For calculation purposes, the index values vs wavelength are usually expressed by a Sellmeier equation or modified Sellmeier equation. Once in this form, the phasematching expression for SHG $n_0^{\omega} = n_e^{2\omega}(\theta)$ can be solved directly for the phasematching angle θ. For three-frequency phasematching conditions, a small computer program is usually written to solve simultaneously the two equations $\omega_3 = \omega_2 + \omega_1$ and $\mathbf{k}_3 = \mathbf{k}_2 + \mathbf{k}_1$ where $\mathbf{k} = 2\pi n(\lambda)/\lambda$. Care must be taken in solving these equations since they may be double valued. The $LiNbO_3$ parametric oscillator tuning curves, shown in Figure 2, were calculated in this manner using analytical expressions for the index of refraction given by Hobden & Warner (153).

Nonlinear crystals must also have a very uniform birefringence over the crystal length for efficient nonlinear conversion. Birefringence uniformity places one of the most stringent requirements on the growth of quality nonlinear crystals. Nash et al (154) have discussed the reduction in conversion efficiency due to birefringent nonuniformities.

Another limitation to nonlinear conversion efficiency is the breaking of phasematching due to thermally induced birefringence changes. This problem has been treated in detail for SHG by Okada & Ieiri (155). They show that the optimum phasematching temperature shifts with increasing average laser power. In crystals with a large birefringence change with temperature, such as ADP and $LiNbO_3$, thermal breaking of phasematching becomes serious at average power levels near 1 W. On the other hand, crystals such as $LiIO_3$ which have a small temperature variation of birefringence can handle much higher average powers.

DAMAGE INTENSITY An important limitation to the maximum nonlinear conversion efficiency is crystal damage due to the input laser intensity. Laser induced damage may be the result of a number of interactions in the material. Ready (156) discusses possible damage mechanisms in a monograph on the effects of high-power laser radiation. Among the mechanisms considered are thermal heating, induced absorption due to multiphoton absorption which leads to heating or to breakdown, stimulated Brillouin scattering, self-focusing, surface preparation, and dielectric breakdown. Thermal heating, in which the temperature rise of the material is proportional to the input pulse duration or deposited energy is a common damage

mechanism in metals and highly absorbing materials. Semiconductors behave more like metals than dielectrics for this form of damage. Ready (156) lists semiconductor damage thresholds (see p. 305 of ref. 156) as energy dependent near 5–10 J/cm^2. For a 100 nsec laser pulse the damage intensity is thus 50–100 MW/cm^2 which agrees with reported values for silicon and germanium (157). For 1 nsec pulses the power density increases by 100 to greater than 1 GW/cm^2 if thermal damage remains the dominant mechanism. There is experimental evidence in GaAs that such high damage thresholds are reached for pulses near 1 nsec. This has important implications for infrared nonlinear optics since, in general, parametric gains are limited by the much lower 20–60 MW/cm^2 damage threshold for long pulses. In the limit of cw pumping, semiconductor materials have damage thresholds as low as 1 kW/cm^2 due to surface heating and melting.

Damage thresholds for dielectric materials are generally much higher than for semiconductors. For example, sapphire damages near 25 GW/cm^2 for Q-switch pulse irradiation. Glass & Guenther (158) have reviewed damage studies in dielectrics. They point out that nonlinear materials show a marked decrease in damage threshold for phasematched second harmonic generation. For example, $LiIO_3$ shows surface damage at 400 MW/cm^2 for 10 nsec pulses. When phasematched it damages at 30 MW/cm^2 for the fundamental and 15 MW/cm^2 for the second harmonic. Similar results have been noted in $LiNbO_3$ and $Ba_2NaNb_5O_{15}$.

In a series of very careful studies, Ammann (159) measured $LiNbO_3$ surface damage thresholds with various quarter wave coatings. He found that uncoated $LiNbO_3$ damages at 40 MW/cm^2 at 1.08 μm for a 0.5 W, 4 kHz, 140 nsec repetitively Q-switch laser source. The damage threshold was increased to 150 MW/cm^2 for a $\lambda/4$ layer of Al_2O_3-coated $LiNbO_3$ crystal. Additional measurements on thin ZnS films showed the importance of overcoating and the lowering of the damage threshold with time upon exposure to air (160). Similar lowering of damage threshold for ThF_2 overcoated CdSe crystals used in an infrared parametric oscillator has been noted (161). In that case the damage threshold decreased from 60 MW/cm^2 to 10 MW/cm^2 over a period of a few days. In addition, damage occurred much more readily along surface scratches, indicating that surface preparation is important.

Bass & Barrett (162) proposed a probabilistic model for laser induced damage based on an avalanche breakdown model. For this damage mechanism, the laser field acts as an ac analog to dc dielectric breakdown. A laser power density of 10 GW/cm^2 corresponds to 4×10^6 V/cm, which is close to the measured dc dielectric breakdown fields near 30×10^6 V/cm. Bass & Barrett (162) have presented the laser damage threshold in a probabilistic way such that the probability to induce surface damage is proportional to $\exp(-K/E)$ where K is a constant and E is the root mean square (rms) optical field strength. Measured dielectric breakdown intensities lie near 25 GW/cm^2 for glasses and fused silica and between 2–4 GW/cm^2 for nonlinear crystals. It appears that if other damage mechanisms to not limit the laser intensity at lower levels, then laser induced dielectric breakdown determines the maximum incident intensity. Efforts to understand the mechanisms of laser induced damage have been increasing (163, 164). Hopefully these studies will lead to a better understanding of the material's damage intensity limits.

Fortunately the damage intensity for most useful nonlinear materials lies between

10 MW/cm^2 and 1 GW/cm^2. Figure 3 then shows that nonlinear conversion efficiencies or parametric gains are high for crystal lengths on the order of 1 cm. The damage intensity does place a limit on the energy handling capabilities of nonlinear crystals. Thus Q-switched laser pulse energies transmitted through 1 cm^2 area crystals are limited to 1–10 J. For most applications of nonlinear crystals this is not a serious limit since the laser host medium and the nonlinear material damage at similar energy densities.

KDP and its Isomorphs

KDP, ADP, and their isomorphs are ferroelectric crystals (165) belonging to the $\bar{4}2m$ tetragonal point group above their Curie temperatures. KDP crystals are transparent from 0.21 to 1.4 μm for the nondeuterated and 0.21 to 1.7 μm for the deuterated material (166). ADP has a similar transparency range. KDP and its isomorphs are negative birefringent and are phasematchable over most of their transparency range. For a complete reference to crystal indices of refraction see Milek & Welles (166), Bechmann & Kurtz (95), and Singh (35).

Because of the availability of large, high optical quality crystals, KDP and ADP were the subject of early nonlinear optical experiments by Miller et al (167) and Miller (21). Later Francois (140) and Bjorkholm & Siegman (141) made accurate cw measurements of ADP's nonlinearity. In addition, Bjorkholm (168) has made comparative nonlinear coefficient measurements of other crystals relative to KDP and ADP.

KDP and ADP have played a significant role as efficient second harmonic generators for both cw and pulsed sources. For cw doubling ADP and KDP can be temperature tuned to the 90° phasematching condition over a limited range of fundamental wavelengths between 0.54 μm and 0.49 μm at temperatures between $+60$°C and -80°C (169, 170). In particular, ADP and KDP 90° phasematch for doubling 5145 Å at -9.2°C and -11.0°C. Other isomorphs of KDP 90° phasematch over different wavelength regions. For example, Rubidium dihydrogen arsenate (RDA) 90° phasematches for doubling the 0.694 μm Ruby laser (171) and Cesium dihydrogen arsenate (CDA) 90° phasematches for doubling 1.06 μm (172).

Using 90° phasematched ADP, Dowley & Hodges (169) obtained up to 100 mW of 2573 Å in 1 msec pulses and 30–50 mW of cw power. The doubling was performed internal to an argon ion laser cavity to take advantage of the high circulating fields. The SHG efficiency was strongly dependent on crystal losses.

The ultraviolet transparency and phasematching characteristics of KDP isomorph crystals make them useful for ultraviolet generation by sum and second harmonic generation. Huth et al (173) were the first to demonstrate this capability by externally doubling a dye laser source. Similarly Yeung & Moore (174) and Sato (175) have generated tunable ultraviolet between 3044–3272 Å by summing a Ruby pumped dye laser and a Ruby laser.

Wallace (176) reported an intracavity doubled dye laser that tunes between 2610 and 3150 Å. This source uses a Q-switched internally doubled Nd:YAG laser as a pump source for the rhodamine 6G and sodium fluorescein dye laser. The ADP intracavity doubled dye laser produced 32 mW of average power at 2900 Å in a

2–3 cm^{-1} bandwidth. The conversion efficiency from input doubled Nd:YAG to ultraviolet power was 4.3%. At the 65° phasematching angle used for doubling the rhodamine 6G dye laser, the ADP double refraction angle is $\rho = 0.025$ rad, which results in a conversion efficiency to the second harmonic of 1% per 100 W of input power.

Using a 1 J per pulse 10 pulse per second Nd:YAG laser source, Yarborough (177) has obtained high ultraviolet pulse energies and average powers. For the 1.06 μm source Yarborough uses a flashlamp pumped 1/4″ diameter rod Nd:YAG oscillator followed by 1/4″ diameter and 3/8″ diameter rod amplifiers. This source is doubled in a 90° phasematched CD*A crystal at 45% efficiency yielding 450 mJ, 0.532 μm pulses. The CD*A phasematches at 103°C and the incident 1.06 μm power is unfocused into the 20 mm CD*A crystal. The green 0.532 μm source is doubled into the ultraviolet in a 2 cm long 90° phasematched ADP crystal. The conversion efficiency for this step is 22%, yielding 100 mJ pulses at 0.266 μm. The harmonic generation in both CD*A and ADP takes place without damage to the crystals. The power levels reported are limited by the laser source becoming unpolarized at high pumping levels. Simultaneously, thermal heating of the doubling crystals begins to limit the second harmonic generation efficiency. The ultraviolet source has been used as a pump for an ADP parametric oscillator (66). In addition, the green output at 0.532 μm has been used to pump dye lasers with up to 60% conversion efficiency.

The high energy, high average power source reported by Yarborough illustrates the optical quality of KDP and its isomorphs. In addition, the use of 90° phasematching for efficient second harmonic generation demonstrates its advantage in these experiments. Although KDP-type crystals have not been utilized extensively in parametric oscillator studies, they play an important role in generating tunable ultraviolet radiation by second harmonic and sum generation of tunable visible sources.

$LiNbO_3$ and $LiIO_3$

$LiNbO_3$ is a ferroelectric material (178) with a Curie temperature approximately 40°C below its melting point of 1253°C. Since the recognition of the unique electro-optical (179) and nonlinear optical (180) properties of $LiNbO_3$ in 1964, it has been extensively studied (181). The growth and physical properties of $LiNbO_3$ have been discussed in a series of papers by Nassau et al (182) and by Abrahams et al (183–185). The electro-optic coefficients for $LiNbO_3$ have been measured by a number of workers (186–189), as have the indices of refraction (153, 190, 191). A particularly useful form for the refractive indices, including temperature dependence, is given by Hobden & Warner (153).

Early work with $LiNbO_3$ showed two potentially troublesome optical properties: optically induced inhomogeneities in the refractive index (11, 192–196) and growth-dependent birefringent variations (197–200). The optically induced index inhomogeneities were found to be self-annealing for crystal temperatures above approximately 180°C for visible radiation and 100°C for near infrared radiation. This fact led to attempts to grow "hot" $LiNbO_3$ by adjusting the composition (198) and by

doping with MgO to increase the birefringence to achieve phasematching for 1.06 μm at temperatures approaching 180°C. In addition, new but related crystals such as $BaNaNb_5O_{15}$ (39, 201) were grown in an attempt to overcome the index damage problem. Unfortunately, these attempts were not successful due to the poor crystal quality that resulted from doping $LiNbO_3$ and to the striations inherent in $Ba_2NaNb_5O_{15}$ crystals.

Although growth striations severely limit the size and quality of $Ba_2NaNb_5O_{15}$ crystals, they have been used to double cw Nd:YAG lasers (39, 202) with good efficiency. The nonlinear coefficient, which is approximately three times that of $LiNbO_3$, partially offsets the disadvantage of smaller crystals of less optical quality. Serious attempts to grow striation-free $Ba_2NaNb_5O_{15}$ crystals have not been successful so that the use of this material is not widespread.

The growth-dependent birefringent variations in $LiNbO_3$ were less difficult to eliminate. The problem was solved by growth of $LiNbO_3$ from its congruent melting composition near a lithium to niobium ratio of 0.48 mole % (203–205). The growth of $LiNbO_3$ crystals from a congruent melt plus improved optical quality tests (199, 206) led to uniform high quality single crystals of over 5 cm in length.

Ferroelectric $LiNbO_3$ has a large variation of birefringence with temperature. This allows SHG at 90° phasematching for fundamental wavelengths between 1 and 3.8 μm at temperatures between 0°C and 550°C. Conversely, $LiNbO_3$ 90° phasematches for parametric oscillation for a number of pump wavelengths and can be temperature tuned over a broad spectral region. Figure 2 shows the parametric oscillator tuning curves for various pump wavelengths of an internally doubled Q-switched Nd:YAG laser. These $LiNbO_3$ phasematching curves were calculated by using the Hobden & Warner (153) index of refraction expressions. Additional $LiNbO_3$ tuning curves, including angular dependence, are given by Harris (79, 207) and Ammann et al (208).

The internally doubled Q-switched Nd:YAG pumped $LiNbO_3$ parametric oscillator is the best developed parametric oscillator at this time. This system is described by Wallace (209). The Nd:YAG laser pump source operates with an internal $LiIO_3$ doubling crystal, acousto-optic Q-switch, and two Brewster angle prisms for wavelength selection. The combination of four doubled Nd:YAG pump wavelengths and temperature tuning allows the oscillator to cover the 0.54 to

Table 1 $LiNbO_3$ parametric oscillator operating parameters

Tuning Range (μm)	Peak Power (W)	Average Power (mW)	Pulse Length (nsec)	Laser Pump Wavelength (μm)
3.50–2.50	80–150	5–10	70	0.532
0.975–2.50	250–350	30	80	0.659
0.725–0.975	250	20	200	0.562
0.623–0.760	250	50	150	0.532
0.546–0.593	300	3–5	200	0.473

3.65 μm spectral region. Table 1 gives the oscillator spectral output wavelengths, laser pump wavelengths, and output power levels. The values used in this table are useful for comparative purposes since they reflect the characteristics of the particular Q-switched Nd:YAG pump laser and are not $LiNbO_3$ oscillator limits.

Threshold for the $LiNbO_3$ SRO with a 5 cm length 90° phasematched crystal is typically between 300 and 600 W. The peak power conversion efficiency is near 50% for an oscillator operating a few times above the threshold. Due to the finite pump pulse width and oscillator build-up time, the energy conversion efficiency is approximately 30%. However, much higher conversion efficiencies have been reported.

$LiNbO_3$ is one of the highest quality nonlinear optical materials. Its use in parametric oscillators to generate tunable radiation over the 0.6 to 3.5 μm spectral range is a demonstration of its importance as a nonlinear material.

In 1968 Kurtz & Perry (142) applied a technique based on the measurement of SHG of powders to the search for nonlinear materials. That search led to the evaluation of α-iodic acid (α-HIO_3) for phasematched second harmonic generation by Kurtz et al (210). Measurement of the nonlinearity of α-HIO_3 showed that it had a nonlinear coefficient approximately equal to that of $LiNbO_3$. The favorable nonlinear properties of α-HIO_3 led to consideration of other AIO_3 crystals (211). One of the first crystals considered was lithium iodate, $LiIO_3$. Its optical and nonlinear optical properties were studied by Nath & Haussuhl (212) and Nash et al (213). The more favorable optical quality of $LiIO_3$ compared to α-HIO_3 has led to its use in a number of nonlinear applications spanning its entire transparency range from 0.35 to 5.5 μm.

$LiIO_3$ (point group 6) has a measured nonlinear coefficient slightly greater than that of $LiNbO_3$ (168, 171, 214, 215). Its indices of refraction and large birefringence ($\Delta n = 0.15$) have been measured as have phasematching angles for various pump wavelengths. $LiIO_3$ phasematches at 52° for doubling 0.6943 μm of a Ruby laser (44, 168, 216) and at 30° for doubling a 1.06 μm Nd:YAG laser.

$LiIO_3$ has proved particularly useful as a high optical quality nonlinear crystal for internal second harmonic generation of a Nd:YAG laser. For this application the laser mirrors are highly reflecting in the infrared but are transparent at the second harmonic. To obtain efficient doubling the laser operates Q-switched. In this mode, the $LiIO_3$ acts as a nonlinear output coupler and efficiently doubles the Nd:YAG. By operating with a prism in the laser cavity any one of 15 Nd:YAG laser lines can be selected and efficiently doubled by rotating the $LiIO_3$ to the phasematching angle. In this way wavelengths at 0.473, 0.532, 0.579, and 0.659 μm can be generated. For example, peak powers of over 10 kW and average powers of greater than 1 W have been obtained from the internally doubled Nd:YAG laser source (72).

In 1970 Campillo & Tang (217) studied spontaneous parametric scattering in $LiIO_3$ and Dobrzhanskii et al (218) carried out similar measurement in α-HIO_2. Shortly afterward, Goldberg (81) constructed a $LiIO_3$ parametric oscillator pumped with a Ruby laser and Izrailenko et al (82) demonstrated an oscillator using $LiIO_3$ and α-HIO_3 pumped by a doubled Nd:Glass laser.

Campillo (219) also externally doubled the $LiIO_3$ oscillator using an 8 mm $LiIO_3$

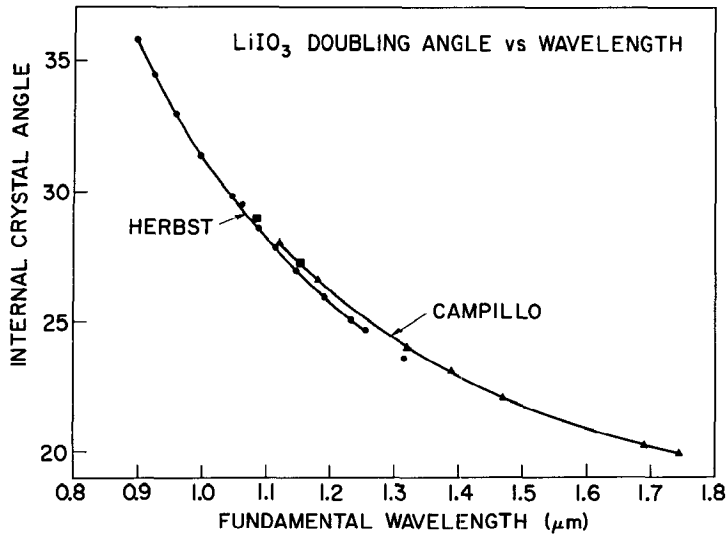

Figure 4 Measured $LiIO_3$ phasematching angles vs fundamental wavelength. Data between 1.1 and 1.8 μm from Campillo (219) and data between 0.9 and 1.3 μm from Herbst (161).

crystal cut at 21.4°. Figure 4 shows the phasematching angles obtained in that experiment over a range of fundamental wavelengths between 1.1 and 1.8 μm. The second harmonic output at 100 W peak power tuned between 0.560 and 0.915 μm. Figure 4 also shows phasematching data obtained by Herbst (161) in an internally doubled $LiNbO_3$ parametric oscillator and illustrates the phasematching properties of $LiIO_3$ for SHG over a broad spectral region.

The infrared transmission of $LiIO_3$ allows interactions out to 5.5 μm. Parametric oscillation is possible, but not useful for idler wavelengths this far in the infrared due to low gain. However, $LiIO_3$ does phasematch for mixing. Meltzer & Goldberg (220) have demonstrated mixing in $LiIO_3$ internal to a Ruby pumped dye laser. Output powers of 100 W were generated over the 4.1 to 5.2 μm region by mixing the Ruby source with the wavelengths from a DTTC dye laser. The spectral width of the dye laser was 6 Å in its 0.802 to 0.835 μm region. Although $LiIO_3$ is transparent and phasematchable in the near infrared spectral region, its low effective nonlinearity due to the 19° phasematching angle reduces its conversion efficiency to the point that other materials may prove more useful for infrared generation by mixing.

Semiconductor Nonlinear Materials

$LiNbO_3$ and $LiIO_3$ parametric oscillators have been tuned to 3.7 and 4.5 μm in the infrared. Infrared oscillation is limited to these wavelengths due to the onset of crystal absorption. Semiconductor nonlinear materials as discussed in this section means the capability of extended infrared tuning from the two-photon absorption

limit to beyond 10 μm. All materials that satisfy this extended infrared transparency range are semiconductors with bandgaps between 2 and 0.5 eV.

Tellurium was an early crystal used for SHG in the infrared (221–223). However, problems in crystal growth and handling have held back its widespread use. Tellurium has the largest nonlinear coefficient $d_{11} = 649 \times 10^{-12}$ m/V of any known crystal, but its large birefringence of $\Delta n = -1.45$ and indices of refraction $n_o = 6.25$, $n_e = 4.80$ make it difficult to use and force phasematching to very small angles. In spite of these difficulties, tellurium has been used to double a 10.6 μm CO_2 laser with 5% efficiency (45). Higher efficiencies were not possible due to induced absorption loss by free electron generation by the intense fundamental and second harmonic waves (45). This problem is intensified in tellurium due to its 4.0 μm bandgap which permits two-photon absorption, thus generating the free carriers which lead to free carrier absorption.

Proustite (Ag_3AsS_3) is an extensively studied infrared nonlinear crystal first considered by Hulme et al (224). Its large birefringence allows phasematched nonlinear interactions over its entire 0.6 to 13 μm transparency range. Proustite has been used to double a 10.6 μm CO_2 laser (225) and to up convert 10.6 μm into the visible using a Ruby laser pump source (49). Its indices of refraction have been measured by Hobden (226). Proustite's large birefringence ($\Delta n = 0.22$) allows off-angle phasematching near $\theta = 20°$. Propagation at such a phasematching angle results in a reduced effective nonlinear coefficient $d_{\text{eff}} = d_{31} \sin\theta + d_{22} \cos\theta$ that is approximately twice d_{31} for $LiNbO_3$. In addition, the large birefringence results in a large double refraction angle ($\rho = 0.08$), giving a short effective interaction length. In spite of these drawbacks and the low crystal burn density near 25 MW/cm^2, proustite has operated as a parametric oscillator near 2.1 μm pumped by a 1.06 μm Q-switched source (227, 228). Recently Hanna et al (229) extended the operation of a proustite parametric oscillator to the singly resonant configuration. They were able to angle tune the oscillator over an extended 1.22 to 8.5 μm spectral range. However, operation of the infrared oscillator in proustite is still marginal due to crystal damage problems and mirror coating problems. These difficulties can be bypassed by mixing in proustite using a near infrared source (56, 57).

In addition to proustite, two closely related crystals have been investigated for infrared nonlinear optical applications. These materials are pyrargyrite (Ag_3SbS_3) (222, 224, 230) and Tl_3AsSe_3 described by Feichtner & Roland (231). Pyrargyrite has properties very similar to proustite. It belongs to the same point group (3m), is transparent between 0.6 and 13 μm and has a large enough birefringence to phasematch over its transparency region. The measured phasematching angle for doubling 10.6 μm is 29°. Its nonlinear coefficient is very close to that of proustite.

The material Tl_3AsSe_3 appears useful as an infrared nonlinear material. Its transparency range extends from 1.26 to 17 μm and the crystal has been grown in sizes up to 1.2 cm diameter and 3 cm in length. The crystal has large birefringence similar to proustite and phasematches for doubling 10.6 μm at 22°. The measured nonlinear coefficient is 3.3 times that of proustite and pyrargyrite. In addition, Feichtner & Roland measured the crystal burn density at 10.6 μm to be 32 MW/cm^2 compared to 20 MW/cm^2 for proustite and 14 MW/cm^2 for pyrargyrite.

Unlike proustite and its related crystals, cadmium selenide (CdSe) 90° phase-matches over an extended infrared region. Wurtzite (6 mm) CdSe does not have adequate birefringence for second harmonic generation; however, it does phase-match for mixing and off-degenerate parametric oscillator operation (79). In addition to its high optical quality, CdSe has a nonlinear coefficient three times that of $LiNbO_3$.

Herbst & Byer (58) performed the first phasematched interaction in CdSe by mixing 10.6 μm against the 1.833 μm Nd:YAG line (232) to generate 2.2 μm. The measured angle for the allowed Type II phasematching was 77°. The observed mixing efficiency was 35% in a 0.6 cm crystal at 48 MW/cm^2, which is less than the measured crystal burn density of 60 MW/cm^2.

The extended 0.75 to 25 μm transparency range of CdSe makes it useful as a tunable mixing source between 8 and 25 μm. In a recent experiment using a $LiNbO_3$ parametric oscillator source, Herbst & Byer (see 86) generated tunable radiation between 10 and 13.5 μm by mixing in CdSe. The measured peak output power of 2 W agreed with the expected conversion efficiency.

In an extension of the mixing experiment in CdSe, Herbst & Byer (83) demonstrated the first singly resonant infrared parametric oscillator in CdSe pumped by the 1.833 μm line of Nd:YAG. Davydov et al (233) also reported achieving singly resonant oscillation in CdSe. The observed threshold for the Herbst-Byer oscillator was 550 W and pump depletions of up to 40% were obtained. Figure 5 is a photo-

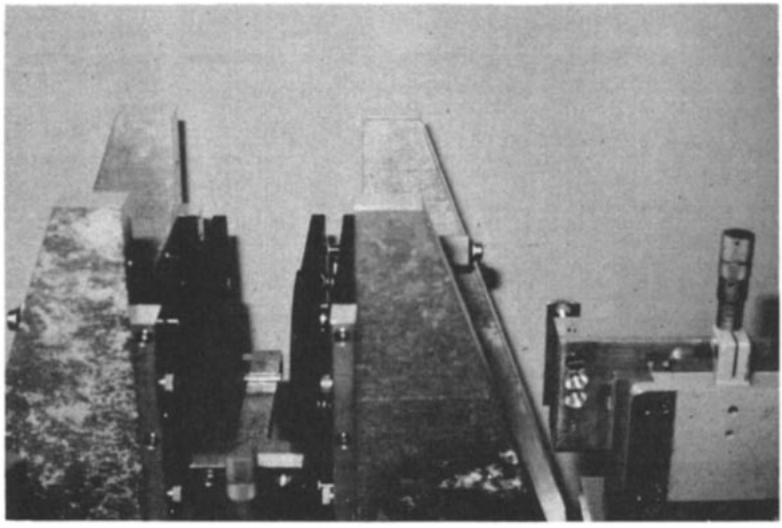

Figure 5 Photograph of a CdSe singly resonant parametric oscillator operating at 2.2 and 10 μm in the infrared. The pump radiation is incident from the right through a lens. The 2 cm long CdSe crystal within the 5.7 μm confocal cavity is rotated for tuning.

graph of the CdSe parametric oscillator showing the 2 cm CdSe crystal within the 5.7 cm confocal cavity. At this time CdSe crystals up to 3 cm in length are commercially available with longer (74 mm) higher-quality crystals having been reported (234). CdSe singly resonant oscillators should operate reliably without crystal burning for 4 cm long crystals.

Considerable effort has gone into growing new nonlinear materials, especially materials that are useful in the infrared. One group of materials with the chalcopyrite ($CuFeS_2$, point group $\bar{4}2m$) structure (235) has particularly useful nonlinear properties.

The chalcopyrite crystals form two groups which are ternary analogs of the II–VI and III–V binary semiconductors. The first group is the I–III–VI_2 compounds of which $AgGaS_2$ and $AgGaSe_2$ are examples. The second group is the II–IV–V_2 compounds which include $CdGeAs_2$ and $ZnGeP_2$. Goryunova et al (236) were the first to investigate the semiconducting and nonlinear optical properties of chalcopyrite crystals. In 1971 Chemla et al (237) reported on $AgGaS_2$ and later that year Boyd et al (238) measured the properties of $ZnGeP_2$ and carried out a phasematched up-conversion experiment of 10.6 μm (52). Byer et al (239) measured the properties of $CdGeAs_2$. The properties of these chalcopyrites and other potentially useful crystals of the same class were extensively studied by Boyd et al (146, 240, 241) in a series of papers. As a result of these and other measurements (125, 242) four crystals belonging to the chalcopyrite semiconductors have been identified as phasematchable and potentially useful for infrared nonlinear optics. These crystals are $CdGeAs_2$, $ZnGeP_2$, $AgGaSe_2$, and $AgGaS_2$.

$AgGaS_2$ is transparent between 0.6 and 13 μm. It is negative birefringent and phasematchable over a wide range of the infrared (237, 240, 241). At this time crystals up to 1 cm in size have been grown, but optical quality is not yet sufficient for use in parametric oscillators. The material has been used for infrared generation by mixing and for second harmonic generation (59).

$AgGaSe_2$ is a close analogy to $AgGaS_2$. However, its transparency range (0.73–17 μm) and phasematching curves are shifted to longer wavelengths. Figure 6 shows the calculated $AgGaSe_2$ tuning curves based on the index of refraction data of Boyd et al (146). Crystals have been recently grown up to 4 cm in length with 0.02 cm^{-1} loss at 10.6 μm. Although $AgGaSe_2$ has not been used in a parametric oscillator, efficient SHG of 10.6 μm and 7–15 μm parametric mixing have been demonstrated (61). $AgGaSe_2$ single crystals grow readily. This, along with its improved optical quality, high nonlinearity, and infrared phasematching, make it a very useful infrared nonlinear material (60).

Unlike the negative birefringent $AgGaS_2$ and $AgGaSe_2$, $ZnGeP_2$ and $CdGeAs_2$ are positive birefringent. Thus the Type II phasematching ($n_p^o \omega_p = n_s^e(\theta)\omega_s + n_i^o \omega_i$) is allowed at 90° where Type I phasematching has a zero effective nonlinear coefficient. However, the effective nonlinearity is maximum for Type I phasematching $[n_p^o \omega_p = n_s^e(\theta)\omega_s + n_i^e(\theta)\omega_i]$ at $\theta = 45°$. Type II phasematching doubles the birefringence needed to achieve phasematching since it averages the birefringence at the longer wavelengths. $ZnGeP_2$ does not have enough birefringence to Type II phasematch for SHG. However, it does phasematch for Type I SHG. Complete Type I

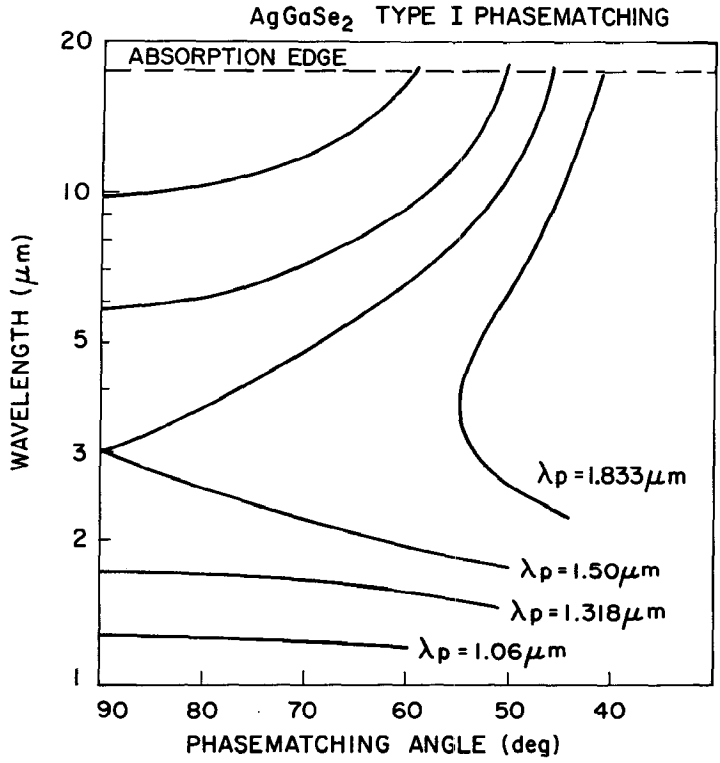

Figure 6 Calculated parametric oscillator tuning curves for $AgGaSe_2$ for various pump wavelengths showing the extended 2–18 μm phasematching range.

SHG phasematching curves for $ZnGeP_2$ are given by Boyd et al (146). $ZnGeP_2$ has been used for infrared up-conversion (52).

$CdGeAs_2$ has the highest parametric figure of merit of any known crystal except Tellurium. In addition, it is particularly useful for SHG of a 10.6 μm CO_2 laser or for parametric oscillation with a 5.3 μm pump source (239). Recent work (46) has demonstrated the potential of $CdGeAs_2$ by SHG of a CO_2 laser with 15% efficiency in a 9 mm length crystal. Phasematched third harmonic generation is also possible in $CdGeAs_2$ (243) and has been extensively studied both theoretically and experimentally (121). $CdGeAs_2$ crystals have been grown up to 9 mm in length with a loss near 0.2 cm^{-1} at 10.6 μm. Crystal size and optical quality improvements are required before the full potential of this material can be realized.

At this time the chalcopyrite crystals satisfy all of the requirements for nonlinear materials except low absorption loss and crystal uniformity. The crystals cannot yet be grown in adequate sizes of high optical quality. However, the very useful nonlinear properties, especially in the infrared, lend considerable importance to chalcopyrite crystal growth efforts.

CONCLUSION

The properties of nonlinear materials are better understood when discussed with reference to nonlinear devices and the theory of nonlinear interactions. Therefore, in the first half of this review, I discussed nonlinear phenomena including the origin of the nonlinear susceptibility and the theoretical models which describe crystal nonlinearity. Nonlinear interactions which were briefly reviewed included second harmonic generation and the three-frequency processes of sum and difference frequency generation and parametric generation and oscillation. The important aspects of focusing and the concept of phasematching were introduced.

With the above discussion as a frame of reference, the nonlinear material requirements including crystal nonlinearity, transparency, birefringence, and damage intensity were discussed. These properties were illustrated by describing useful nonlinear crystals. The properties of KDP and ADP, $LiNbO_3$, $LiIO_3$, and semiconductor materials including proustite, pyrargyrite, cadmium selenide, and four chalcopyrite materials were summarized. For reference Table 2 lists the linear and nonlinear properties of selected nonlinear materials.

The first column of Table 2 gives the presently accepted values for the crystal nonlinear coefficients. These values are based upon Levine & Bethea's (244) best value for GaAs. The parametric gain is proportional to the material parameters $d^2/n_0^2 n_3$ where d is the effective nonlinear coefficient at the angle of phasematching and n_0 and n_3 are the indices of refraction for the degenerate and pump waves. Column 8 of Table 2 lists the material figure of merit which is also shown in Figure 1 along with the crystal transparency range.

In many applications the pump laser has more than adequate power. In this case the quantity of interest is the nonlinear conversion efficiency per input intensity and the crystal burn intensity. The calculated conversion efficiency $\Gamma^2 l^2$ given in Table 2 assumes a 1 cm length crystal unless stated otherwise. Figure 3 shows the conversion efficiency at 1 MW/cm^2 pump intensity for the crystals listed in Table 2. The four chalcopyrite crystals and $LiNbO_3$ and ADP show good efficiencies. An important limitation to the maximum parametric gain is the material damage. Table 2 lists approximate values for damage in nonlinear crystals based on reported damage intensity measurements. Since laser induced damage may be the result of a number of interactions in the material, the reported values vary widely. However, the listed values are useful for estimating the conversion efficiency of a nonlinear crystal as limited by the onset of damage.

The properties of a large number of nonlinear materials have been measured and useful nonlinear crystals for the ultraviolet, visible, and infrared regions have been characterized. Although the nonlinear crystals listed in Table 2 allow nonlinear interactions over the spectral range from 0.25 to 25 μm, there are large classes of materials that have not been investigated. Among these are organic materials (245) and crystals potentially useful in the ultraviolet at wavelengths less than 0.2 μm.

There remains considerable work yet to be done for the full theoretical understanding of nonlinear crystals and the growth and improvement of presently known phasematchable crystals. However, progress since the first experiment of Franken

Table 2 Nonlinear coefficient, figure of merit, conversion efficiency, burn intensity,

Material (point group pump wavelength)	$d \times 10^{12}$ (m/V) (References)	n_o n_e	$n_e - n_o$	θ_m	ρ	$d_{\text{eff}} \times 10^{12}$
Te (32) $\lambda_p = 5.3\ \mu$m	$d_{11} = 649$ (222)	6.25 4.80	−1.45	14°	0.10	638 ($d \cos^2 \theta_m$)
$CdGeAs_2$ ($\bar{4}2m$) $\lambda_p = 5.3\ \mu$m	$d_{36} = 236$ (241, 239)	3.51 3.59	+0.086	II 55°	0.021	193 ($d \sin\theta$)
				I 35°	0.021	212 ($d \sin 2\theta$)
GaAs ($\bar{4}3m$)	$d_{36} = 90.1$ (244)	3.30	0	—	—	—
$ZnGeP_2$ ($\bar{4}2m$) $\lambda_p = 1.83\ \mu$m	$d_{36} = 75$ (238)	3.11 3.15	+0.038	II 90°	0.0	d_{36}
				I 62°	0.01	62.2 ($d \sin 2\theta$)
Tl_3AsSe_3 ($3m$) $\lambda_p = 1.83\ \mu$m	$d_+ = 40$ (231)	3.34 3.15	−0.182	36°	0.055	d_+
$AgGaSe_2$ ($\bar{4}2m$) $\lambda_p = 1.83\ \mu$m	$d_{36} = 33$ (146)	2.62 2.58	−0.32	I 55°	0.01	27 ($d \sin\theta$)
				I 90°	0.0	d_{36}
CdSe (6 mn) $\lambda_p = 1.83\ \mu$m	$d_{31} = 19$ (238, 58)	2.45 2.47	+0.019	90°	0.0	d_{31}
$AgGaSe_2$ ($\bar{4}2m$) $\lambda_p = 0.946\ \mu$m	$d_{36} = 12$ (240)	2.42 2.36	−0.054	I 64°	0.17	10.8 ($d \sin\theta$)
				I 90°	0.0	d_{36}
Ag_3SbS_3 ($3m$) $\lambda_p = 1.06\ \mu$m	$d_+ = 12$ (222)	2.86 2.67	−0.19	—	—	d_+
Ag_3AsS_3 ($3m$) $\lambda_p = 1.06\ \mu$m	$d_+ = 11.6$ (231)	2.76 2.54	−0.223	30°	0.078	d_+
$LiIO_3$ (6) $\lambda_p = 0.694\ \mu$m	$d_{31} = 7.5$ (214)	1.85 1.72	−0.135	23°	0.071	3.04 ($d \sin\theta$)
$LiNbO_3$ ($3m$) $\lambda_p = 0.532$	$d_{31} = 6.25$ (137)	2.24 2.16	−0.081	90°	0.0	d_{31}
ADP ($\bar{4}2m$) $\lambda_p = 0.266$	$d_{36} = 0.57$ (140, 141)	1.53 1.48	−0.0458	90°	0.0	d_{36}
KDP ($\bar{4}2m$) $\lambda_p = 0.266$	$d_{36} = 0.50$ (143)	1.51 1.47	−0.0417	90°	0.0	d_{36}
SiO_2 (32)	$d_{11} = 0.33$ (143)	1.55 1.56	+0.0095	—	—	d_{11}

and transmission range for nonlinear crystals

$d_{eff}^2/n_0^2 n_3 \times 10^{24}$	$l(\rho)_{eff}$ (cm)	$\Gamma^2 l^2$ (1 W)	$\Gamma^2 l^2$ (1 MW/cm^2)	I_{burn} (MW/cm^2)	Transmission Range (μm)
3634	0.011	0.95×10^{-4}	0.18	40–60	4–25
861	0.34	3.8×10^{-4}	0.033	20–40	2.4–17
1039		4.6×10^{-4}	0.040		
226	$l_{coh} = 104\ \mu$m	—	—	60	0.9, 1.4 – 17
187	$l = 1$ cm	7.1×10^{-3}	0.21	>4	0.7–12
127	0.59	1.8×10^{-3}	0.05		
51	0.019	3.7×10^{-5}	0.022	32	1.2–18
42	0.71	5.52×10^{-4}	0.02	>10	0.73–17
63.4	$l = 1$ cm	1.98×10^{-3}	0.07		
24	$l = 2$ cm	1.3×10^{-3}	0.09	60	0.75–25
9.2	0.14	2.3×10^{-4}	0.013	12–25	0.60–13
11	$l = 1$ cm	2.3×10^{-3}	0.045		
7.6	—	8.2×10^{-6}	0.01	14–50	0.60–14
8.2	0.007	9.0×10^{-6}	0.011	12–40	0.60–13
1.88	0.008	5.6×10^{-6}	5.5×10^{-3}	125	0.31–5.5
3.88	$l = 5$ cm	2.1×10^{-2}	1.28	50–140	0.35–4.5
0.100	$l = 5$ cm	2.9×10^{-3}	0.131	>1000	0.20–1.1
0.079	$l = 5$ cm	2.30×10^{-3}	0.103	>1000	0.22–1.1
0.029	$l_{coh} = 14\ \mu$	—	—	>1000	0.18–3.5

et al (1) has been rapid. I would like to conclude this review by suggesting what lies ahead in tunable coherent sources based on nonlinear interactions in crystals. The parametric oscillator is a unique tunable coherent source because its gain mechanism due to the crystal nonlinearity is independent of its tuning and bandwidth, which depend on the crystal birefringence and dispersion. Where tunable laser sources typically operate over a 10% bandwidth (a dye laser for example) the parametric oscillator tunes over a greater than two to one range. As an example, Figure 7 shows the tuning curve of a 1.06 μm pumped $LiNbO_3$ parametric oscillator which angle tunes between 1.5 μm and 4.0 μm. This oscillator was recently demonstrated (246) and is capable of rapid tuning and high output energies.

The $LiNbO_3$ parametric oscillator's basic tuning range can be extended toward the infrared by mixing the signal and idler in $AgGaSe_2$ to cover the 3–18 μm range and by mixing in CdSe to tune over the 10–30 μm range. Second harmonic generation in $LiNbO_3$ and in $LiIO_3$ extends the tuning to 0.3–1.5 μm. Finally, sum generation

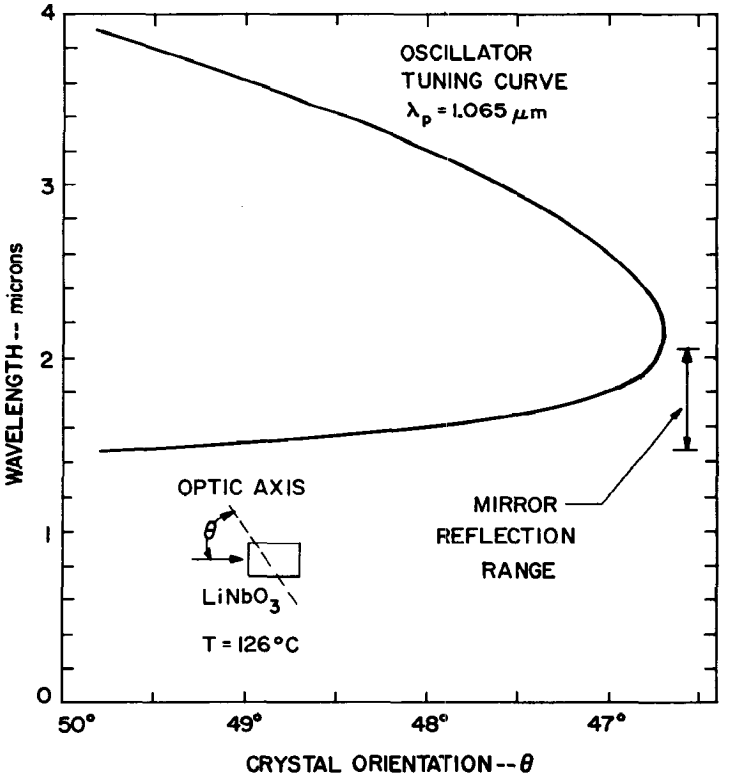

Figure 7 Tuning curve for a 1.06 μm Nd:YAG pumped $LiNbO_3$ parametric oscillator. The mirror reflectance range for singly resonant operation is indicated.

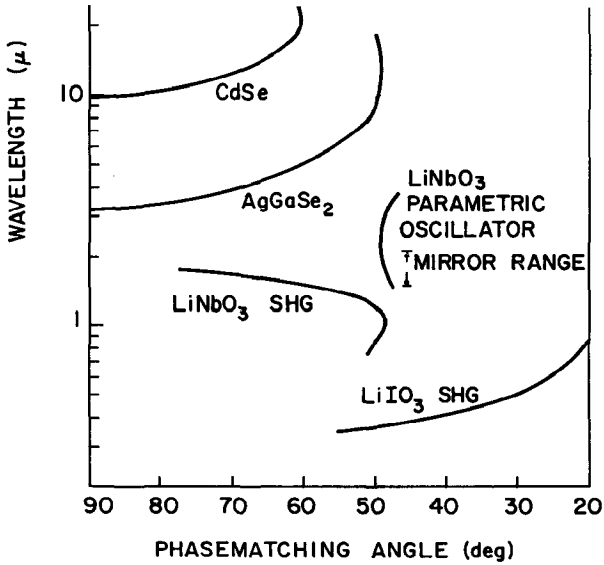

Figure 8 Spectral range vs crystal phasematching angle for the 1.06 μm Nd:YAG pumped $LiNbO_3$ parametric oscillator and following nonlinear crystal generators. CdSe and $AgGaSe_2$ phasematch for infrared generation by mixing the $LiNbO_3$ oscillator's signal and idler frequencies. $LiNbO_3$ and $LiIO_3$ phasematch for doubling the primary oscillator frequency range into the visible and ultraviolet.

in ADP phasematches for generation of 0.22–0.3 μm in the ultraviolet. Figure 8 illustrates the phasematching angles and tuning ranges for these nonlinear interactions. A detailed study (247) shows that for 10 mJ pump energies available from a 1.06 μm *Q*-switched Nd:YAG laser source, the parametric oscillator and all following nonlinear interactions are 10–30% efficient. This widely tunable, high energy device should operate very much like a coherent spectrometer source. The spectrometer concept illustrates the unique capabilities of nonlinear interactions for generation of coherent radiation over an extended spectral range. The efficiency and high power capability of nonlinear interactions assure wider application of nonlinear devices as future tunable coherent sources.

Literature Cited

1. Franken, P. A., Hill, A. E., Peters, C. W., Weinreich, G. 1961. *Phys. Rev. Lett.* 7:118
2. Kleinman, D. A. 1962. *Phys. Rev.* 126: 1977
3. Giordmaine, J. A. 1962. *Phys. Rev. Lett.* 8:19
4. Maker, P. D., Terhune, R. W., Nisenoff, N., Savage, C. M. 1962. *Phys. Rev. Lett.* 8:21
5. Akhmanov, S. A., Kovrigin, A. I., Khoklov, R. V., Chunaev, O. N. 1963. *Zh. Eksp. Teor. Fiz.* 45:1336. Transl. 1964. *Sov. Phys. JETP* 18:919
6. Bjorkholm, J. E. 1966. *Phys. Rev.* 142: 126

7. Kleinman, D. A., Ashkin, A., Boyd, G. D. 1966. *Phys. Rev.* 145:338
8. Bloembergen, N., Pershan, P. S. 1962. *Phys. Rev.* 128:606
9. Kleinman, D. A. 1962. *Phys. Rev.* 128: 1761
10. Boyd, G. D., Ashkin, A., Dziedzic, J. M., Kleinman, D. A. 1965. *Phys. Rev. A* 137:1305
11. Ashkin, A. et al 1966. *Appl. Phys. Lett.* 9:72
12. Akhmanov, S. A., Dmitriev, V. G., Modenov, V. P. 1965. *Radiotekh. Elektron.* 10:649. Transl. 1965. *Radio Eng. Electron. Phys.* 10:552
13. Wright, J. K. 1963. *Proc. IEEE* 51:1663
14. Smith, R. G., Nassau, K., Galvin, M. F. 1965. *Appl. Phys. Lett.* 7:256
15. Wang, C. C., Racette, G. W. 1965. *Appl. Phys. Lett.* 6:169
16. Kingston, R. H. 1962. *Proc. IRE* 50: 472
17. Kroll, N. M. 1962. *Phys. Rev.* 127:1207
18. Akhmanov, S. A., Khokhlov, R. V. 1962. *Zh. Eksp. Teor. Fiz.* 43:351. Transl. 1963. *Sov. Phys. JETP* 16:252
19. Armstrong, J. A., Bloembergen, N., Ducuing, J., Pershan, P. S. 1962. *Phys. Rev.* 127:1918
20. Giordmaine, J. A., Miller, R. C. 1965. *Phys. Rev. Lett.* 14:973
21. Miller, R. C. 1964. *Appl. Phys. Lett.* 5: 17
22. Akhmanov, S. A., Khokhlov, R. V. 1964. *Problems in Nonlinear Optics.* Moscow: Akad. Nauk SSR. English ed. 1973. N.Y.: Gordon and Breach
23. Bloembergen, N. 1965. *Nonlinear Optics.* New York: Benjamin
24. Butcher, P. N. 1965. *Nonlinear Optical Phenomena.* Columbus, Ohio: Ohio State Univ.
25. Franken, P. A., Ward, J. F. 1963. *Rev. Mod. Phys.* 35:23
26. Ovander, L. N. 1965. *Sov. Phys. Usp.* 8:337
27. Bonch-Bruevich, A. M., Khodovoi, V. A. 1965. *Sov. Phys. Usp.* 8:1
28. Minck, R. W., Terhune, R. W., Wang, C. C. 1966. *Appl. Opt.* 5:1595
28a. Pershan, P. S. 1966. In *Progress in Optics,* ed. E. Wolf, 5:85 114. New York: Interscience, Amsterdam: North Holland
29. Akhmanov, S. A. et al 1967. *Parametric Generators of Light.* Presented at the Symp. Mod. Opt., Polytechnic Institute of Brooklyn, Brooklyn, New York, March, 1967
30. Terhune, R. W., Maker, P. D. 1968. In *Advances in Lasers,* ed. A. K. Levine, 2:295–370. New York: Dekker
31. Akhmanov, S. A., Khokhlov, R. V. 1968. *Sov. Phys. Usp.* 11:394
32. Kielich, S. 1970. *Opt. Electron.* 2:125
33. Suvorov, V. S., Sonin, A. S. 1967. *Sov. Phys. Crystallogr.* 11:711–23
34. Rez, I. S. 1968. *Sov. Phys. Usp.* 10: 759–82
34a. Hulme, K. F. 1973. *Rep. Progr. Phys.* 36:497–540
35. Singh, S. 1971. In *Handbook of Lasers,* ed. R. J. Pressley. Chem. Rubber Co. Press. p. 489
36. Baldwin, G. C. 1969. *An Introduction to Nonlinear Optics.* New York: Plenum
37. Zernike, F., Midwinter, J. E. 1973. *Applied Nonlinear Optics.* New York: Academic
38. Rabin, H., Tang, C. L. *Treatise in Quantum Electronics.* New York: Academic (to be published)
39. Geusic, J. E., Levinstein, H. J., Rubin, J. J., Singh, S., van Uitert, L. G. 1968. *Appl. Phys. Lett.* 11:269; see also Geusic, J. E., Levinstein, H. J., Singh, S., Smith, R. G., van Uitert, L. G. 1968. *Appl. Phys. Lett.* 12:306
40. Dowley, M. W. 1968. *Appl. Phys Lett.* 13:395
41. Hagen, W. F., Magnante, P. C. 1969. *J. Appl. Phys.* 40:219
42. Chesler, R. B., Karr, M. A., Geusic, J. E. 1970. *J. Appl. Phys.* 41:4125
43. Wallace, R. W. 1972. *IEEE J. Quantum Electron.* 8:819
44. Nath, G., Mehmanesch, H., Gsaenger, M. 1970. *Appl. Phys. Lett.* 17:286
45. Gandrud, W. B., Abrams, R. L. 1970. *Appl. Phys. Lett.* 7:302
46. Kildal, H., Mikkelsen, J. C. 1974. *Opt. Commun.* In press
47. Smith, H. A., Mahr, H. 1970. *An Infrared Detector for Astronomy Using Up-Conversion Techniques.* Presented at the Int. Quantum Electron. Conf., Kyoto, Japan, September 1970
48. Boyd, G. D., Bridges, T. J., Burkhardt, E. G. 1968. *IEEE J. Quantum Electron.* 4:515
49. Warner, J. 1968. *Appl. Phys. Lett.* 12: 222
50. Gandrud, W. B., Boyd, G. D. 1969. *Opt. Commun.* 1:187
51. Klinger, Y., Abrams, F. R. 1969. *Proc. IEEE* 57:1797
52. Boyd, G. D., Gandrud, W. B., Buehler, E. 1971. *Appl. Phys. Lett.* 18:446
52a. Boyd, G. D., Bridges, T. J., Patel, C. K. N., Buehler, E. 1972. *Appl. Phys. Lett.* 21:553
53. Midwinter, J. E. 1968. *IEEE J. Quantum Electron.* 4:716
54. Andrews, R. A. 1970. *IEEE J. Quantum*

Electron. 6:68
55. Zernike, F., Berman, P. R. 1965. *Phys. Rev. Lett.* 15:999
56. Hanna, D. C., Smith, R. C., Stanley, C. R. 1971. *Opt. Commun.* 4:300
57. Decker, C. D., Tittel, F. K. 1973. *Opt. Commun.* 8:244
58. Herbst, R. L., Byer, R. L. 1971. *Appl. Phys. Lett.* 19:527
59. Hanna, D. C., Rampal, V. V., Smith, R. C. 1973. *Opt. Commun.* 8:151
60. Kildal, H., Mikkelsen, J. C. 1973. *Opt. Commun.* 9:315
61. Byer, R. L., Choy, M. M., Herbst, R. L., Chemla, D. S., Feigelson, R. S. 1974. *Appl. Phys. Lett.* 24:65
62. Louisell, W. H. 1960. *Coupled Mode and Parametric Electronics.* New York: Wiley
63. Yariv, A., Pearson, J. E. 1969. In *Progress in Quantum Electronics,* ed. J. H. Sanders, K. W. H. Stevens, 1:1–49. New York: Pergamon
64. Akhmanov, S. A. et al 1966. *JETP Lett.* 3:241
65. Akmanov, A. G. et al 1968. *IEEE J. Quantum Electron.* 4:828
66. Yarborough, J. M., Massey, G. A. 1971. *Appl. Phys. Lett.* 18:438
67. Giordmaine, J. A., Miller, R. C. 1966. *Physics of Quantum Electronics,* ed. P. L. Kelley, B. Lax, P. E. Tannenwald, 31–42. New York: McGraw; also, 1965. *Proc. Phys. Quantum Electron. Conf.,* San Juan, Puerto Rico, June 28–30, 1965
68. Giordmaine, J. A., Miller, R. C. 1966. *Appl. Phys. Lett.* 9:298
69. Bjorkholm, J. E. 1968. *Appl. Phys. Lett.* 13:53
70. Falk, J., Murray, J. E. 1969. *Appl. Phys. Lett.* 14:245
71. Ammann, E. O., Foster, J. D., Oshman, M. K., Yarborough, J. M. 1969. *Appl. Phys. Lett.* 15: 131
72. Wallace, R. W., Harris, S. E. 1970. *Laser Focus* p. 42
73. Smith, R. G., Geusic, J. E., Levinstein, H. J., Singh, S., Van Uitert, L. G. 1968. *J. Appl. Phys.* 39:4030
74. Smith, R. G. et al 1968. *Appl. Phys. Lett.* 12:308
75. Laurence, C., Tittel, F. 1971. *J. Appl. Phys.* 42:2137
76. Weller, J. F., Giallorenzi, T. G., Andrews, R. A. 1972. *J. Appl. Phys.* 43:4650
77. Byer, R. L., Oshman, M. K., Young, J. F., Harris, S. E. 1968. *Appl. Phys. Lett.* 13:109
78. Byer, R. L., Kovrigin, A. I., Young, J. F. 1969. *Appl. Phys. Lett.* 15:136
79. Harris, S. E. 1969. *Proc. IEEE* 57:2096
80. Wallace, R. W. 1971. *IEEE Conference on Laser Applications. Washington, D.C. 1971*
81. Goldberg, L. S. 1970. *Appl. Phys. Lett.* 17:489
82. Izrailenko, A. I., Kovrigin, A. I., Nikles, P. V. 1970. *JETP Lett.* 12:331
83. Herbst, R. L., Byer, R. L. 1972. *Appl. Phys. Lett.* 21:189
84. Smith, R. G. 1973. *Advances in Lasers,* ed. A. K. Levine, A. J. DeMaria, Vol. 4. In press
85. Byer, R. L. 1973. In *Treatise in Quantum Electronics,* ed. H. Rabin, C. L. Tang. New York: Academic. In press
86. Byer, R. L. 1973. *Parametric Oscillators, Proc. Tunable Laser Spectrosc. Conf., 1st,* Vail, Colorado, June 1973. To be published
87. Bass, M., Franken, P. A., Ward, J. F., Weinreich, G. 1962. *Phys. Rev. Lett.* 9:446
88. Terhune, R. W., Maker, P. D., Savage, C. M. 1962. *Phys. Rev. Lett.* 8:404
89. Kaiser, W., Garrett, C. G. B. 1961. *Phys. Rev. Lett.* 7:229
90. Eckhart, G. et al 1962. *Phys. Rev. Lett.* 9:455
91. Chiao, R. Y., Townes, C. H., Stoicheff, B. P. 1964. *Phys. Rev. Lett.* 12:592
92. Mash, D. I., Morozov, V. V., Starunov, V. S., Fabelinskii, I. L. 1965. *JETP Lett.* 2:22
93. Wemple, S. H., DiDomenico, M. Jr. 1972. In *Applied Solid State Science,* ed. R. Wolfe, Vol. 3. New York: Academic
93a. Ducuing, J., Flytzanis, C. 1970. In *Optical Properties of Solids,* ed. F. Abeles. Amsterdam: North Holland
94. Nye, J. F. 1960. *Physical Properties of Crystals,* Chap. VII. London: Oxford Univ. Press
95. Bechmann, R., Kurtz, S. K. 1969. *Landolt-Bornstin Numerical Data and Functional Relationships in Science and Technology New Series Group III,* ed. K. H. Hellwege, A. M. Hellwege, 2: 167–209. Berlin: Springer Verlag
96. Pershan, P. S. 1963. *Phys. Rev.* 130:919
97. Boyd, G. D., Kleinman, D. A. 1968. *J. Appl. Phys.* 39:3597
98. Lax, B., Mavroides, J., Edwards, D. 1962. *Phys. Rev. Lett.* 8:166
99. Garrett, C. G. B., Robinson, F. N. H. 1966. *IEEE J. Quantum Electron.* 2: 328
100. Kurtz, S. K., Robinson, F. N. H. 1967. *Appl. Phys. Lett.* 10:62
101. Butcher, P. N., McLean, T. O. 1963. *Proc. Phys. Soc.* 81:219
102. Kelley, P. L. 1963. *J. Phys. Chem. Solids* 21:607

103. Cheng, H., Miller, P. B. 1964. *Phys. Rev. A* 134:683
104. Ward, J. F. 1965. *Rev. Mod. Phys.* 37:1
105. Miles, R. B., Harris, S. E. 1973. *IEEE J. Quantum Electron.* 9:470
106. Robinson, F. N. H. 1967. *Bell Syst. Tech. J.* 46:913
107. Flytzanis, C. 1968. *C.R. B* 267:555
108. Flytzanis, C., Ducuing, J. 1969. *Phys. Rev.* 178:1218
109. Jha, S., Bloembergen, N. 1968. *Phys. Rev.* 171:891
110. Phillips, J. C., Van Vechten, J. A. 1969. *Phys. Rev.* 183:709
111. Van Vechten, J. A., Phillips, J. C. 1970. *Phys. Rev. B* 2:2160
112. Penn, D. 1962. *Phys. Rev.* 128:2093
113. Levine, B. F. 1969. *Phys. Rev. Lett.* 22:789
114. Levine, B. F. 1970. *Phys. Rev. Lett.* 25:440
115. Levine, B. F. 1973. *Phys. Rev. Lett. B* 7:2591, 2600
116. Kleinman, D. A. 1970. *Phys. Rev. B* 2:3139
117. Chemla, D. S. 1971. *Phys. Rev. Lett.* 26:1441
118. Tang, C. L., Flytzanis, C. 1971. *Phys. Rev. B* 4:2520
119. Tang, C. L. 1973. *IEEE J. Quantum Electron.* 9:755
120. Chemla, D. S. 1972. *Ann. Telecommun.* 27:11–12
121. Chemla, D. S., Begley, R. F., Byer, R. L. 1974. *IEEE J. Quantum Electron.* 10:71
122. Kurtz, S. K. 1973. In *Laser Handbook*, ed. F. T. Arecchi, E. O. Schulz-DuBois, 923–74. Amsterdam: North Holland
123. Hobden, M. V. 1967. *J. Appl. Phys.* 38:4365
124. Bey, P. P., Tang, C. L. 1972. *IEEE J. Quantum Electron.* 8:361
125. Kildal, H. 1972. PhD thesis. Stanford University, Stanford, California. (Available as Microwave Laboratory Report No. 2118)
126. Harris, S. E., Carson, D., Young, J. F. 1972. Private communication
127. Warner, J. 1971. *Opt. Electron.* 3:37
128. Andrews, R. A. 1970. *IEEE J. Quantum Electron.* 6:68
129. Kleinman, D. A., Boyd, G. D. 1969. *J. Appl. Phys.* 40:546
130. Boyd, G. D., Ashkin, A. 1966. *Phys. Rev.* 146:187
131. Akhmanov, S. A., Sukhorukov, A. P., Khokhlov, R. V. 1967. *Usp. Fiz. Nauk* 93:19. Transl. 1968. *Sov. Phys. Usp.* 10:609
132. Rabson, T. A., Ruiz, H. J., Shah, P. L., Tittle, F. K. 1972. *Appl. Phys. Lett.* 21:129
133. Harris, S. E., Oshman, M. K., Byer, R. L. 1967. *Phys. Rev. Lett.* 18:732
134. Magde, D., Mahr, H. 1967. *Phys. Rev. Lett.* 18:905
135. Byer, R. L. 1968. PhD thesis. Stanford University, Stanford, California.
136. Giordmaine, J. A. 1969. *Phys. Today* 22:38
137. Byer, R. L., Harris, S. E. 1968. *Phys. Rev.* 168:1064
138. Giallorenzi, T. G., Tang, C. L. 1968. *Phys. Rev.* 166:225
139. Kleinman, D. A. 1968. *Phys. Rev.* 174:1027
140. Francois, G. E. 1966. *Phys. Rev.* 143:597
141. Bjorkholm, J. E., Siegman, A. E. 1967. *Phys. Rev.* 154:851
142. Kurtz, S. K., Perry, T. T. 1968. *J. Appl. Phys.* 39:3798
143. Jerphagnon, J., Kurtz, S. K. 1970. *J. Appl. Phys.* 41:1667; see also Jerphagnon, J., Kurtz, S. K. 1970. *Phys. Rev. B* 1:1738
144. Wynne, J. J., Bloembergen, N. 1969. *Phys. Rev.* 188:1211
145. Chemla, D. S., Kupecek, P. 1971. *Rev. Phys. Appl.* 6:31
146. Boyd, G. D., Kasper, H. M., McFee, J. H., Storz, F. G. 1972. *IEEE J. Quantum Electron.* 8:900
147. Byer, R. L. 1970. *Opt. Spectra* 42
148. Kleinman, D. A., Miller, R. C., Nordland, W. A. 1973. *Appl. Phys. Lett.* 23:243
149. Donnay, J. D. H., Donnay, G. 1963. *Crystal Data.* American Crystallographic Assoc. 2nd ed.
150. Winchell, A. N., Winchell, H. 1964. *Optical Properties of Artificial Minerals.* New York: Academic
151. Wemple, S. H. 1969. *Phys. Rev. Lett.* 23:1156
152. Wemple, S. H., DiDomenico, M. Jr. 1969. *J. Appl. Phys.* 40:735
153. Hobden, M. V., Warner, J. 1966. *Phys. Lett.* 22:243
154. Nash, F. R., Boyd, G. D., Sargent, M. III, Bridenbaugh, P. M. 1970. *J. Appl. Phys.* 41:2564
155. Okada, M., Ieiri, S. 1971. *IEEE J. Quantum Electron.* 7:560
156. Ready, J. F. 1971. *Effects of High Power Laser Radiation.* New York: Academic
157. Hanna, D. C., Luther-Davies, B., Rutt, H. N., Smith, R. C., Stanley, C. R. 1972. *IEEE J. Quantum Electron.* 8:317
158. Glass, A. J., Guenther, A. H. 1972.

Appl. Opt. 11:832
159. Ammann, E. O. 1972. *Technical Report AFAL-TR-72-177, Air Force Avionics Laboratory, Wright Patterson AFB, Ohio*
160. Ammann, E. O., Wintemute, J. D. 1973. *J. Opt. Soc. Am.* 63:965
161. Herbst, R. L. 1973. Private communication
162. Bass, M., Barrett, H. H. 1972. *IEEE J. Quantum Electron.* 8:338
163. Giuliano, C. R. 1972. *IEEE J. Quantum Electron.* 8:749
164. Bass, M., Fradin, D. W. 1973. *IEEE J. Quantum Electron.* 9:890
165. Jona, F., Shirane, G. 1962. *Ferroelectric Crystals.* New York: McMillan
166. Milek, J. T., Welles, S. J. 1970. *Linear Electro-Optic Modulator Materials.* Electronic Properties Information Center, Hughes Aircraft Company
167. Miller, R. C., Kleinman, D. A., Savage, A. 1963. *Phys. Rev. Lett.* 11:146
168. Bjorkholm, J. E. 1968. *IEEE J. Quantum Electron.* 4:970, and correction to above, *IEEE J. Quantum Electron.* 5:260
169. Dowley, M. W., Hodges, E. B. 1968. *IEEE J. Quantum Electron.* 4:552
170. Huth, B. G., Kiang, Y. C. 1969. *J. Appl. Phys.* 40:4976
171. Pearson, J. E., Evans, G. A., Yariv, A. 1972. *Opt. Commun.* 4:366
172. Adhav, R. S., Wallace, R. W. 1973. *IEEE J. Quantum Electron.* 9:854
173. Huth, B. G., Farmer, G. I., Taylor, L. M., Kagan, M. R. 1968. *Spectrosc. Lett.* 1:425
174. Yeung, E. S., Moore, C. B. 1971. *J. Am. Chem. Soc.* 93:2059
175. Sato, T. 1972. *J. Appl. Phys.* 43:1837
176. Wallace, R. W. 1971. *Opt. Commun.* 4:316
177. Yarborough, J. M. 1972. Private communication
178. Matthias, B. T., Remeika, J. P. 1949. *Phys. Rev.* 76:1886
179. Peterson, G. E., Ballman, A. A., Lenzo, P. V., Bridenbaugh, P. M. 1964. *Appl. Phys. Lett.* 5:62
180. Boyd, G. D., Miller, R. C., Nassau, K., Bond, W. L., Savage, A. 1964. *Appl. Phys. Lett.* 5:234
181. Miller, R. C., Boyd, G. D., Savage, A. 1965. *Appl. Phys. Lett.* 6:77
182. Nassau, K., Levinstein, H. J., Loiacono, G. M. 1966. *J. Phys. Chem. Solids* 27:983, 989
183. Abrahams, S. C., Reddy, J. M., Bernstein, J. L. 1966. *J. Phys. Chem. Solids* 27:997
184. Abrahams, S. C., Hamilton, W. C., Ready, J. M. 1966. *J. Phys. Chem. Solids* 27:1013
185. Abrahams, S. C., Levinstein, H. J., Ready, J. M. 1966. *J. Phys. Chem. Solids* 27:1019
186. Lenzo, P. V., Spencer, E. G., Nassau, K. 1966. *J. Opt. Soc. Am.* 56:633
187. Turner, E. H. 1966. *Appl. Phys. Lett.* 8:303
188. Zook, J. D., Chen, D., Otto, G. N. 1967. *Appl. Phys. Lett.* 11:159
189. Hulme, K. F., Davies, P. H., Cound, V. M. 1969. *J. Phys. C* 2:855
190. Miller, R. C., Savage, A. 1966. *Appl. Phys. Lett.* 9:169
191. Boyd, G. D., Bond, W. L., Carter, H. L. 1967. *J. Appl. Phys.* 48:1941
192. Chen, F. S. 1969. *J. Appl. Phys.* 40:3389
193. Johnston, W. D. Jr. 1970. *J. Appl. Phys.* 41:3279
194. Angert, N. B., Pisskov, V. A., Solov'eva, N. M. 1972. *Sov. Phys. JETP* 35:867
195. Wood, V. E. 1973. *J. Appl. Phys.* 44:1391
196. Serreze, H. B., Goldner, R. B. 1973. *Appl. Phys. Lett.* 22:629
197. Bergman, J. G. et al 1968. *Appl. Phys. Lett.* 12:92
198. Fay, H., Alford, W. J., Dess, H. M. 1968. *Appl. Phys. Lett.* 12:89
199. Midwinter, J. E. 1968a. *Appl. Phys. Lett.* 11:128
200. Miller, R. C., Nordland, W. A., Bridenbaugh, P. M. 1971. *J. Appl. Phys.* 42:4145
201. Byer, R. L., Harris, S. E., Kuizenga, D. J., Young, J. F., Feigelson, R. S. 1969. *J. Appl. Phys.* 40:444
202. Kerr, M. A. 1971. *J. Appl. Phys.* 42:4517
203. Lerner, P., Legras, C., Dumas, J. P. 1968. *Crystal Growth, 1968 Proc. Second Int. Conf. Crystal Growth Birmingham, U.K., July 1968,* ed. F. C. Frank, J. B. Mullin, H. S. Peiser, 231. Amsterdam: North Holland
204. Carruthers, J. R., Peterson, G. E., Grasso, M., Bridenbaugh, P. M. 1971. *J. Appl. Phys.* 42:1846
205. Midwinter, J. E. 1968. *J. Appl. Phys.* 39:3033
206. Byer, R. L., Young, J. F., Feigelson, R. S. 1970. *J. Appl. Phys.* 41:2320
207. Harris, S. E. 1969. *Chromatix Tech. Lett. No. 1*
208. Ammann, E. O., Yarborough, J. M., Falk, J. 1971. *J. Appl. Phys.* 42:5618
209. Wallace, R. W. 1970. *Appl. Phys. Lett.* 17:497
210. Kurtz, S. K., Perry, T. T., Bergman,

J. G. Jr. 1968. *Appl. Phys. Lett.* 12: 186
211. Bergman, J. G., Boyd, G. D., Ashkin, A., Kurtz, S. K. 1969. *J. Appl. Phys.* 40:2860
212. Nath, G., Haussuhl, S. 1969. *Appl. Phys. Lett.* 14:154
213. Nash, F. R., Bergman, J. G. Jr., Boyd, G. D., Turner, E. H. 1969. *J. Appl. Phys.* 40:5201
214. Campillo, A. J., Tang, C. L. 1971. *Appl. Phys. Lett.* 19:36
215. Jerphagnon, J. 1970. *Appl. Phys. Lett.* 16:298
216. Nath, G., Haussuehl, S. 1969. *Phys. Lett. A* 29:91
217. Campillo, A. J., Tang, C. L. 1970. *Appl. Phys. Lett.* 16:242; see also 1968. *Appl. Phys. Lett.* 12:376
218. Dobrzhanskii, G. F. et al 1970. *JETP Lett.* 12:353
219. Campillo, A. J. 1972. *IEEE J. Quantum Electron.* 8:809
220. Meltzer, D. W., Goldberg, L. S. 1972. *Opt. Commun.* 5:209
221. Patel, C. K. N. 1966. *Phys. Rev. Lett.* 16:613
222. McFee, J. H., Boyd, G. D., Schmidt, P. H. 1970. *Appl. Phys. Lett.* 17:57
223. Sherman, G. H., Coleman, P. D. 1973. *IEEE J. Quantum Electron.* 9:403
224. Hulme, K. F., Jones, O., Davies, P. H., Hobden, M. V. 1967. *Appl. Phys. Lett.* 10:133
225. Boggett, D. M., Gibson, A. F. 1968. *Phys. Lett. A* 28:33
226. Hobden, M. V. 1969. *Opt. Electron.* 1:159
227. Ammann, E. O., Yarborough, J. M. 1970. *Appl. Phys. Lett.* 17:233
228. Hanna, D. C., Luther-Davies, B., Rutt, H. N., Smith, R. C. 1972. *Appl. Phys. Lett.* 20:34
229. Hanna, D. C., Luther-Davies, B., Smith, R. C. 1973. *Appl. Phys. Lett.* 22:440
230. Gandrud, W. B., Boyd, G. D., McFee, J. H., Wehmeier, F. H. 1970. *Appl. Phys. Lett.* 16:59
231. Feichtner, J. D., Roland, G. W. 1972. *Appl. Opt.* 11:993
232. Wallace, R. W. 1971. *IEEE J. Quantum Electron.* 7:203
233. Davydov, A. A., Kulevskii, L. A., Prokhorov, A. M., Savel'ev, A. D., Smirnov, V. V. 1972. *JETP Lett.* 15: 513
234. Abagyan, S. A., Ivanov, G. A., Kartushina, A. A., Koroleva, G. A. 1972. *Sov. Phys. Semicond.* 5:1452
235. Parthe, E. 1964. *Crystal Chemistry of Tetrahedral Structures.* New York: Gordon and Breach
236. Goryunova, N. A., Ryvkin, S. M., Fishman, I. M., Shpen'kov, G. P., Yaroshetskii, I. D. 1965. *Sov. Phys. Semicond.* 2:1272; see also, Goryunova, N. A. 1965. *The Chemistry of Diamond Like Semiconductors.* Cambridge, Mass.: M.I.T. Press
237. Chemla, D. S., Kupccek, P. J., Robertson, D. S., Smith, R. C. 1971. *Opt. Commun.* 1:29
238. Boyd, G. D., Buehler, E., Storz, F. G. 1971. *Appl. Phys. Lett.* 18:301
239. Byer, R. L., Kildal, H., Feigelson, R. S. 1971. *Appl. Phys. Lett.* 19:237
240. Boyd, G. D., Kasper, H., McFee, J. H. 1971. *IEEE J. Quantum Electron.* 7: 563
241. Boyd, G. D., Buehler, E., Storz, F. G., Wernick, J. H. 1972. *IEEE J. Quantum Electron.* 8:419
242. Bahr, G. C., Smith, R. C. 1972. *Phys. Status Solidi* 13:157
243. Kildal, H., Begley, R. F., Choy, M. M., Byer, R. L. 1972. *J. Opt. Soc. Am.* 62: 1398
244. Levine, B. F., Bethea, C. G. 1972. *Appl. Phys. Lett.* 20:272
245. Jerphagnon, J. 1972. Private communication
246. Byer, R. L. 1973. *Tunable Infrared Sources.* Presented at the Opt. Soc. Am. Meet., Rochester, New York, Oct. 1973
247. Byer, R. L., Herbst, R. L. 1973. Manuscript

CONTENTS